AN OVERLAPPING SCHWARZ ALGORITHM FOR ALMOST INCOMPRESSIBLE ELASTICITY[*]

CLARK R. DOHRMANN[†] AND OLOF B. WIDLUND[‡]

Abstract. Overlapping Schwarz methods are extended to mixed finite element approximations of linear elasticity which use discontinuous pressure spaces. The coarse component of the preconditioner is based on a low-dimensional space previously developed for scalar elliptic problems and a domain decomposition method of iterative substructuring type, i.e., a method based on nonoverlapping decompositions of the domain, while the local components of the preconditioner are based on solvers on a set of overlapping subdomains. A bound is established for the condition number of the algorithm which grows in proportion to the logarithm of the number of degrees of freedom in individual subdomains and, essentially, to the third power of the relative overlap between the overlapping subdomains, and which is independent of the Poisson ratio as well as jumps in the Lamé parameters across the interface between the subdomains. A positive definite reformulation of the discrete problem makes the use of the standard preconditioned conjugate gradient method straightforward. Numerical results, which include a comparison with problems of compressible elasticity, illustrate the findings.

Key words. domain decomposition, overlapping Schwarz, preconditioners, iterative methods, almost incompressible elasticity, mixed finite element methods

AMS subject classifications. 65F10, 65N30, 65N55

DOI. 10.1137/080724320

1. Introduction. The subject of this paper is an overlapping Schwarz algorithm for almost incompressible elasticity problems. Previous theory for overlapping Schwarz methods has been restricted to compressible cases in which the Poisson ratio ν is bounded away from its maximum possible value of $1/2$; see [35, section 8]. Here we remove this restriction and present a coarse space which effectively accommodates all values of $\nu < 1/2$. This coarse space is an extension of a component of an iterative substructuring method developed over a decade ago for scalar elliptic problems; see [18] and also [35, Algorithm 5.16]. Recent applications of such extended coarse spaces to a variety of different problem types appear in [14]. We note that the coarse space presented here has already been used successfully as part of a production-level iterative solver in the parallel structural dynamics code Salinas [4].

An early application of overlapping Schwarz methods to mixed formulations of linear elasticity and Stokes problems is given in Klawonn and Pavarino [24]. In that work, the coarse spaces were based on the same mixed finite element methods on coarse meshes and both continuous and discontinuous pressure spaces were considered. An analysis of these methods was not provided, but their performance was shown to be quite competitive with block diagonal and block triangular preconditioners; see [25].

Related iterative substructuring approaches for either incompressible or almost incompressible problems appear in [17, 21, 30, 29]. For each of these methods, special care is required to ensure that the coarse space is properly constructed. As a result, standard coarse spaces for compressible problems must be modified and enriched to accommodate incompressible or almost incompressible cases. The coarse space presented in this paper can be applied without modification to both compressible and almost incompressible cases. In addition, our approach does not require access to individual subdomain matrices; i.e., we can work directly with a globally assembled matrix. One disadvantage of the present algorithm, when compared with the iterative substructuring methods cited above, is the appearance of a cubic factor of the relative overlap between subdomains in the condition number estimate. Although this factor can lead to much larger condition numbers if not controlled, we have not found it to be a limitation in practice.

We restrict our attention in the present work to finite elements with discontinuous pressure interpolation. By doing so, it is possible to eliminate the pressure unknowns at the element level. An important consequence is that the same algorithm, as for compressible elasticity, can be used for almost incompressible cases, since the assembled matrix is symmetric and positive definite, and the method of preconditioned conjugate gradients can be used as the iterative method. We also note that we can use standard finite element methods in any subdomain that is compressible assuming, as always, that the interface nodes match across the interface.

In addition to almost incompressible elasticity, we hope that our work will have an impact on the development of penalty-based and augmented Lagrangian preconditioners for saddle-point systems as in [2, 3, 12, 16]. In particular, we have found in numerical experiments that the present work is relevant to the practical implementation of such preconditioners for incompressible Stokes and Navier–Stokes equations. This is the case because the algorithm presented here effectively handles cases of ν approaching $1/2$, i.e., the incompressible limit.

An overview of mixed finite elements for elasticity is given in section 2. Section 3 is devoted to the development of Lemma 3.3, which is central to the proof of our main result. This lemma, and properties of the chosen coarse space, allow us to apply some existing theory for compressible problems to almost incompressible cases. The proof of our main result, a condition number bound for the algorithm, is provided in section 5. In section 6, we consider the extension of our results to subdomains with boundaries which are not very regular, basing the discussion on our recent work [15, 26]. The paper concludes with supporting numerical examples and a discussion in section 7.

2. Almost incompressible elasticity and mixed finite elements. Let $\Omega \subset \mathbb{R}^n, n = 2, 3$, be a domain with a Lipschitz boundary, and let $\partial\Omega_D$, be a nonempty subset of its boundary $\partial\Omega$, and introduce the Sobolev space $\mathbf{V} := \{\mathbf{v} \in \mathbf{H}^1(\Omega) : \mathbf{v}|_{\partial\Omega_D} = 0\}$. Here $\mathbf{H}^1(\Omega) := H^1(\Omega)^n$. The linear elasticity problem consists in finding the displacement $\mathbf{u} \in \mathbf{V}$ of the domain Ω, fixed along $\partial\Omega_D$ and subject to a surface force of density $\mathbf{g}$, along $\partial\Omega_N = \partial\Omega \setminus \partial\Omega_D$, and a body force $\mathbf{f}$:

$$(2.1) \qquad 2\int_\Omega \mu \, \epsilon(\mathbf{u}) : \epsilon(\mathbf{v}) \, dx + \int_\Omega \lambda \, \mathrm{div} \, \boldsymbol{u} \, \mathrm{div} \, \boldsymbol{v} \, dx \; = \; \langle \mathbf{F}, \mathbf{v} \rangle \quad \forall \mathbf{v} \in \mathbf{V}.$$

Here $\lambda(x)$ and $\mu(x)$ are the Lamé parameters, $\epsilon_{ij}(\mathbf{u}) = \frac{1}{2}(\frac{\partial u_i}{\partial x_j} + \frac{\partial u_j}{\partial x_i})$ is the linearized strain tensor, and two inner products are defined by

$$\epsilon(\mathbf{u}) : \epsilon(\mathbf{v}) = \sum_{i=1}^n \sum_{j=1}^n \epsilon_{ij}(\mathbf{u})\epsilon_{ij}(\mathbf{v}), \; \langle \mathbf{F}, \mathbf{v} \rangle \; = \; \int_\Omega \sum_{i=1}^n f_i v_i \, dx + \int_{\partial\Omega_N} \sum_{i=1}^n g_i v_i \, dA.$$

The Lamé parameters can be expressed in terms of the Poisson ratio ν and Young's modulus E:

$$\lambda = \frac{E\nu}{(1+\nu)(1-2\nu)}, \quad \mu = \frac{E}{2(1+\nu)}.$$

The domain Ω is partitioned into nonoverlapping subdomains Ω_i. In section 6, we will discuss the regularity required of their boundaries for our arguments to be valid. We assume, for simplicity, that the Lamé parameters are constant in each subdomain. Since much of our analysis will be carried out for one subdomain at a time, we can then work with problems with constant coefficients. The bound for the condition number of our algorithm will be independent of the values of all these parameters.

2.1. A saddle-point formulation. When the material becomes almost incompressible, the Poisson ratio ν approaches the value $1/2$ and $\lambda/\mu = 2\nu/(1-2\nu)$ approaches infinity. In such cases, finite element discretizations of this pure displacement formulation will increasingly suffer from locking and very slow convergence of the finite element solution.

A well-known remedy is based on introducing the new variable $p = -\lambda \text{div } \boldsymbol{u} \in U \subset L^2(\Omega)$, which we will call pressure, and replacing the pure displacement problem (2.1) with a mixed formulation: find $(\mathbf{u}, p) \in \mathbf{V} \times U$ such that

$$(2.2) \quad \begin{cases} 2 \int_\Omega \mu \, \epsilon(\mathbf{u}) : \epsilon(\mathbf{v}) \, dx & - & \int_\Omega \text{div } \boldsymbol{v} \, p \, dx & = & \langle \mathbf{F}, \mathbf{v} \rangle & \forall \mathbf{v} \in \mathbf{V}, \\ \\ - \int_\Omega \text{div } \boldsymbol{u} \, q \, dx & - & \int_\Omega 1/\lambda \, pq \, dx & = & 0 & \forall q \in U; \end{cases}$$

see Brezzi and Fortin [9] or Brenner and Scott [8].

In the case of homogeneous Dirichlet boundary conditions for $\mathbf{u}$ on all of $\partial\Omega$, we will choose $U := L_0^2(\Omega) := \{q \in L^2(\Omega) : \int_\Omega q dx = 0\}$, since it follows from the divergence theorem that the pressure will have a zero mean value. For nonzero Dirichlet boundary data, the same is true if the net flux satisfies $\int_{\partial\Omega} \mathbf{u} \cdot \mathbf{n} \, ds = 0$, where $\mathbf{n}$ is the outward normal. If, on the other hand, the boundary conditions are mixed (part essential and part natural), then there is always a unique solution with a pressure component in $U = L^2(\Omega)$. Rather than discussing two somewhat different cases, we will, from now on, focus on the case with homogeneous Dirichlet boundary conditions on all of $\partial\Omega$.

The net fluxes $\int_{\partial\widetilde{\Omega}} \mathbf{u} \cdot \mathbf{n} \, dA$, across the boundary $\partial\widetilde{\Omega}$ of subsets $\widetilde{\Omega}$ of individual subdomains, will be important in our analysis. Only if they vanish are there divergence-free extensions of the boundary values for which the bilinear form $\int_{\widetilde{\Omega}} \lambda \, \text{div } \boldsymbol{u} \, \text{div } \boldsymbol{v} \, dx$ will then vanish.

In our analysis, we will work only with the restrictions of (2.2) to individual subdomains Ω_i or subsets of such subdomains. In such cases, we can factor out the constants μ and $1/\lambda$, and we will use the notation $a_i(\mathbf{u}, \mathbf{v}), b_i(\mathbf{v}, p)$, and $c_i(p, q)$ for the three resulting bilinear forms associated with the subdomain Ω_i.

We note that

$$(\text{div } \boldsymbol{v}, \text{div } \boldsymbol{v})_{L^2(\Omega_i)} \leq n \int_{\Omega_i} \epsilon(\mathbf{v}) : \epsilon(\mathbf{v}) \, dx = n/2 \, a_i(\mathbf{v}, \mathbf{v}), \quad n = 2, 3.$$

Therefore,

$$(2.3) \quad |b_i(\mathbf{v}, p)| = \left| - \int_{\Omega_i} \text{div } \boldsymbol{v} \, p \, dx \right| \leq \sqrt{n/2} a_i(\mathbf{v}, \mathbf{v})^{1/2} c_i(p, p)^{1/2}.$$

In the absence of essential boundary conditions, the elasticity operator has zero energy modes, which are the rigid body modes. There are three of them for $n = 2$ and six for $n = 3$; see further section 4.

By letting $\lambda/\mu \to \infty$, we obtain the limiting problem for incompressible linear elasticity and also a formulation of the Stokes system for incompressible fluids. A penalty term, as in the compressible case, could also originate from stabilization techniques or penalty formulations for Stokes problems.

A Korn inequality for the subspace orthogonal to the rigid body modes will establish an equivalence between the square of the $\mathbf{H}^1(\Omega_i)$-seminorm and the bilinear form $a_i(\cdot, \cdot)$; see section 5 and, in particular, Lemma 5.2. This will make it possible to use many tools and results developed in studies of scalar elliptic problems.

2.2. Finite element methods with discontinuous pressures. We assume that the domain Ω is decomposed into N nonoverlapping subdomains Ω_i of diameter H_i. The interface of this decomposition is given by

$$\Gamma = \left(\bigcup_{i=1}^{N} \partial \Omega_i \right) \setminus \partial \Omega.$$

To simplify our discussion, we will assume that, as in [35, Assumption 4.3], each subdomain is the union of shape-regular triangular or tetrahedral elements of a global conforming coarse mesh and that the number of such triangles or tetrahedra forming any individual subdomain is uniformly bounded. In section 6, we will explore the extent to which this assumption can be relaxed. Each subdomain is further partitioned into many shape-regular elements. We will assume that the nodes match across the interface between the subdomains.

In our experimental work, we have chosen to work with the $Q_2(h) - P_1(h)$ finite elements: the displacement space is $\mathbf{V}^h := (Q_2(h))^n$, where Q_2 is the space of continuous, bi- or triquadratic, tensor product polynomials. The pressure space consists of discontinuous, piecewise linear functions:

$$U^h := \{ q \in U : q|_T \in P_1(T) \ \ \forall T \in \tau_h \}.$$

The two spaces are defined on the same quadrilateral or hexahedral mesh. This mixed finite element method satisfies a uniform inf-sup condition:

$$(2.4) \qquad \sup_{\mathbf{v} \in \mathbf{V}^h} \frac{b_i(\mathbf{v}, q)}{a_i(\mathbf{v}, \mathbf{v})^{1/2}} \geq \beta c_i(q, q)^{1/2} \ \ \forall q \in U^h \cap L_0^2, \ \ \beta > 0.$$

For a proof of the inf-sup stability of this mixed finite element space, see Boffi and Gastaldi [5] or Girault and Raviart [20, pp. 156–158]. The parameter β depends on the domain, and, in particular, it varies inversely with the aspect ratio of the domain; see section 5. There are optimal $O(h^2)$ error estimates for both displacements and pressures for this mixed finite element method provided that *unmapped* linear functions are used for the pressure space; see [5].

We note that while finite element methods based on hexahedra and quadrilaterals enjoy popularity, our theory applies equally well to any stable mixed method, e.g., one based on tetrahedra or triangles as long as the pressure space is discontinuous. We could also consider some more general saddle-point problems with penalty terms.

3. Analysis of saddle-point problems. Consider the linear system

$$(3.1) \qquad \begin{bmatrix} \mu A & B^T \\ B & (-1/\lambda)C \end{bmatrix} \begin{bmatrix} u \\ p \end{bmatrix} = \begin{bmatrix} f \\ 0 \end{bmatrix},$$

corresponding to a stable, mixed finite element formulation of the elasticity problem on a subdomain Ω_i; to simplify, we drop the index i in this section. Here u is the vector of nodal values of the vector valued finite element function $\mathbf{u}(x)$, etc. From (2.3) and with A the stiffness matrix corresponding to $a_i(\cdot, \cdot)$, etc., we find

$$(3.2) \qquad (p^T B u)^2 \leq (n/2)(u^T A u)(p^T C p).$$

Setting $p = \lambda C^{-1} B u$ in (3.2) then gives, after canceling a common factor,

$$(3.3) \qquad u^T B^T C^{-1} B u \leq (n/2) u^T A u.$$

We note that $u^T B^T C^{-1} B u$ can also be written as $\int_{\Omega_i} |\text{div } \mathbf{u}|^2 \, dx$.

The energy of u is defined as $u^T \widetilde{A} u$, where

$$(3.4) \qquad \widetilde{A} = \mu A + \lambda B^T C^{-1} B,$$

a Schur complement obtained by eliminating the variable p; we will also work with a bilinear form $\widetilde{a}_i(\cdot, \cdot)$ which corresponds to this displacement-only formulation. We next partition the displacement vector into

$$(3.5) \qquad u = \left[\begin{array}{c} u_I \\ u_\Gamma \end{array} \right].$$

Here the subscripts I and Γ refer to internal and interface, respectively, and we see that (3.1) can be expressed equivalently as

$$(3.6) \qquad \left[\begin{array}{ccc} \mu A_{II} & \mu A_{I\Gamma} & B_I^T \\ \mu A_{\Gamma I} & \mu A_{\Gamma\Gamma} & B_\Gamma^T \\ B_I & B_\Gamma & (-1/\lambda)C \end{array} \right] \left[\begin{array}{c} u_I \\ u_\Gamma \\ p \end{array} \right] = \left[\begin{array}{c} f_I \\ f_\Gamma \\ 0 \end{array} \right].$$

For $p \in L_0^2$, we obtain from (2.4), and a standard argument,

$$(3.7) \qquad p^T B_I A_{II}^{-1} B_I^T p \geq \beta^2 p^T C p,$$

where β is the discrete inf-sup constant.

From the divergence theorem, we have

$$(3.8) \qquad \int_{\Omega_i} \text{div } \mathbf{u} \, dx = \int_{\partial \Omega_i} (\mathbf{u} \cdot \mathbf{n}) \, dS = g^T u_\Gamma,$$

where $\mathbf{n}$ is the unit outward normal for $\partial \Omega_i$ and g is a constant vector associated with the net flux of $\mathbf{u}$ across $\partial \Omega_i$. We will use a vector valued function of constant divergence defined by

$$(3.9) \qquad \mathbf{v}(x) = \frac{g^T u_\Gamma}{n|\Omega_i|} \sum_{j=1}^n x_j \mathbf{e}_j,$$

where x_j and $\mathbf{e}_j$ are the coordinate and unit vector, respectively, for direction j. The corresponding vector of nodal values will be denoted by v.

We find that

$$(3.10) \qquad \int_{\Omega_i} \text{div } \mathbf{v} \, dx = \int_{\Omega_i} \text{div } \mathbf{u} \, dx.$$

Consequently, since div $\boldsymbol{v}$ is a constant,

$$(3.11) \qquad (\lambda/|\Omega_i|)v_\Gamma^T gg^T v_\Gamma = \lambda \int_{\Omega_i} |\text{div } \boldsymbol{v}|^2 \, dx \le \lambda \int_{\Omega_i} |\text{div } \boldsymbol{u}|^2 \, dx$$

and

$$(3.12) \qquad g^T v_\Gamma = \int_{\partial\Omega_i} (\boldsymbol{v} \cdot \boldsymbol{n}) \, dS = \int_{\partial\Omega_i} (\boldsymbol{u} \cdot \boldsymbol{n}) \, dS = g^T u_\Gamma.$$

Furthermore, by (3.3) and (3.9),

$$u^T(A/2)u = \int_{\Omega_i} \epsilon(\boldsymbol{u}) : \epsilon(\boldsymbol{u}) \, dx \ge (1/n) \int_{\Omega_i} |\text{div } \boldsymbol{u}|^2 \, dx$$

$$\ge (1/n) \int_{\Omega_i} |\text{div } \boldsymbol{v}|^2 \, dx$$

$$(3.13) \qquad \qquad = \int_{\Omega_i} \epsilon(\boldsymbol{v}) : \epsilon(\boldsymbol{v}) \, dx,$$

and we obtain

$$(3.14) \qquad v^T A v \le u^T A u$$

and

$$(3.15) \qquad v^T \widetilde{A} v = \frac{\lambda + 2\mu/n}{|\Omega_i|} u_\Gamma^T gg^T u_\Gamma \le u^T \widetilde{A} u.$$

Now let

$$(3.16) \qquad w_\Gamma = u_\Gamma - v_\Gamma;$$

it follows that $g^T w_\Gamma = 0$; i.e., the net flux across $\partial\Omega_i$ of $\mathbf{w}$ is zero.

We return to (3.6) for (w, q) and consider the case with $f_I = 0$ and w_Γ given. We then obtain

$$(3.17) \qquad \begin{bmatrix} \mu A_{II} & B_I^T \\ B_I & (-1/\lambda)C \end{bmatrix} \begin{bmatrix} w_I \\ q \end{bmatrix} = \begin{bmatrix} -\mu A_{I\Gamma} w_\Gamma \\ -B_\Gamma w_\Gamma \end{bmatrix}.$$

In addition, the mean value $\int_{\Omega_i} q\,dx/|\Omega_i|$ of q is zero as a consequence of $g^T w_\Gamma = 0$ and the divergence theorem. Therefore, although B_I is rank deficient with a null space of dimension 1, the linear system in (3.17) is consistent even for $1/\lambda = 0$. Elimination of w_I gives

$$(3.18) \qquad ((\mu/\lambda)C + B_I A_{II}^{-1} B_I^T)q = \mu(B_\Gamma - B_I A_{II}^{-1} A_{I\Gamma})w_\Gamma,$$

and it then follows from (3.17) and (3.18) that

$$(3.19) \qquad w^T \widetilde{A} w = \mu w_\Gamma^T S_{\Gamma\Gamma} w_\Gamma + \mu w_\Gamma^T \widetilde{B}_\Gamma^T S_{\mu,\lambda}^{-1} \widetilde{B}_\Gamma w_\Gamma,$$

where

$$(3.20) \qquad S_{\Gamma\Gamma} = A_{\Gamma\Gamma} - A_{\Gamma I} A_{II}^{-1} A_{I\Gamma}, \quad \widetilde{B}_\Gamma = B_\Gamma - B_I A_{II}^{-1} A_{I\Gamma},$$

and

$$(3.21) \qquad S_{\mu,\lambda} = (\mu/\lambda)C + B_I A_{II}^{-1} B_I^T.$$

We will use minimal energy extensions with respect to $\widetilde{A}$ and A.

DEFINITION 3.1. *The discrete saddle-point harmonic function for boundary data* w_Γ *has the vector representation*

$$w_{sh} = \left[\begin{array}{c} w_I \\ w_\Gamma \end{array} \right],$$

where w_I *is given by the solution of* (3.17).

DEFINITION 3.2. *The discrete harmonic function for boundary data* w_Γ *has the vector representation*

$$\widehat{w} = \left[\begin{array}{c} -A_{II}^{-1} A_{I\Gamma} \\ I \end{array} \right] w_\Gamma.$$

We can then rewrite (3.19) as

$$(3.22) \qquad w^T \widetilde{A} w = \mu \widehat{w}^T A \widehat{w} + \mu \widehat{w}^T B^T S_{\mu,\lambda}^{-1} B \widehat{w}.$$

It then follows from (3.3), (3.7), and the definition of $S_{\mu,\lambda}$ that

$$(3.23) \qquad w^T \widetilde{A} w \leq \left(1 + \frac{n/2}{\mu/\lambda + \beta^2} \right) \mu \widehat{w}^T A \widehat{w}.$$

Therefore, the energy of the discrete saddle-point harmonic function for the boundary data w_Γ is bounded by a constant times that of the discrete harmonic function with respect to the μA norm. This result will allow us to work with the benign μA norm, even as λ approaches infinity, for displacement fields which satisfy a zero net flux condition. For general displacement fields, we have the following.

LEMMA 3.3. *Let* u_{sh} *denote the discrete saddle-point harmonic function with the same boundary data* u_Γ *as* u. *Then,*

$$(3.24) \qquad u_{sh}^T \widetilde{A} u_{sh} \leq 4 \left(1 + \frac{n/2}{\mu/\lambda + \beta^2} \right) \mu u^T A u + \frac{2(\lambda + 2\mu/n)}{|\Omega_i|} u_\Gamma^T g g^T u_\Gamma.$$

Proof. With $u = v + w$, we find, by using (3.23), (3.16), (3.14), and (3.15), that

$$\begin{aligned} u^T \widetilde{A} u &\leq 2(v^T \widetilde{A} v + w^T \widetilde{A} w) \\ &\leq 2(v^T \widetilde{A} v + (1 + (n/2)/(\mu/\lambda + \beta^2)) \mu \widehat{w}^T A \widehat{w}) \\ &\leq 2(v^T \widetilde{A} v + 2(1 + (n/2)/(\mu/\lambda + \beta^2)) \mu (v^T A v + u^T A u)) \\ (3.25) \qquad &\leq 4(1 + (n/2)/(\mu/\lambda + \beta^2)) \mu u^T A u + 2(\lambda + 2\mu/n)/|\Omega_i| u_\Gamma^T g g^T u_\Gamma. \end{aligned}$$

The lemma then follows from observing that $u_{sh}^T \widetilde{A} u_{sh} \leq u^T \widetilde{A} u$, since u_{sh} minimizes the energy with respect to $\widetilde{A}$ for the boundary data u_Γ. □

4. The algorithm and the main result. We will describe and analyze our algorithm as a two-level Schwarz method, as in [35, Chapters 2 and 3], defined in terms of a set of subspaces. To simplify the discussion, we will consider only the case when exact solvers are used for both the coarse problem and the local problems. We will

work with the displacement variables only and with the positive definite formulation obtained after all pressure degrees of freedom have been eliminated. We will use a coarse space $\mathbf{V}_0$ and a number of local spaces $\mathbf{V}_i'$ associated with an overlapping covering $\{\Omega_i'\}$ of Ω. We will assume that each Ω_i' is constructed by adding layers of elements to a subdomain Ω_i. While other recipes have been considered, this is the most popular approach. We also assume that all finite element nodes for the displacement, which belong to an element with at least one node on an edge of a subdomain Ω_i, belong to Ω_i'; in case we have nodes interior to the elements and nodes in the interior to the subdomain faces, e.g., as for the Q_2 elements, we can relax this condition and require only that we have at least one additional layer of elements in the extended subdomain Ω_i'.

The overlap between the subdomains is characterized by parameters δ_i, somewhat differently from [35, Assumption 3.1]: δ_i is the minimal distance from any face $\mathcal{F}^{i\ell} \subset \partial\Omega_i$, common to Ω_i and a neighboring subdomain Ω_ℓ, to $\partial\Omega_\ell'$.

The coarse component space of our preconditioner is adapted from an earlier iterative substructuring algorithm [35, Algorithm 5.16] first developed for scalar elliptic problems in [18]. Because of the larger null space of the elasticity operator, we need to enrich that coarse space to make it work for elasticity. This is related to the well-known null space property, which is necessary to obtain scalability, i.e., a bound on the convergence, which does not depend on the number of subdomains; see the discussion in [31] or [33]. We build the local components of our preconditioner by restricting the original problem to the overlapping subdomains Ω_i'.

To introduce the coarse space $\mathbf{V}_0$, we first decompose the interface Γ. For problems in the plane, the interface is the union of edges and vertices. An edge $\mathcal{E}^{ij}$ is an open subset of $\Gamma_i := \partial\Omega_i \cap \Gamma$, which contains all nodes which are shared by the boundaries of only a pair of subdomains Ω_i and Ω_j. The subdomain vertices $\mathcal{V}^{i\ell}$ are endpoints of edges and typically are shared by more than two subdomains.

In three dimensions, Γ_i is the union of faces $\mathcal{F}^{ij}$, edges $\mathcal{E}^{ik}$, and vertices $\mathcal{V}^{i\ell}$. A node on a face is common to two subdomains Ω_i and Ω_j, while those on an edge typically are common to more than two. We will call the union of the edges and vertices of a subdomain Ω_i its *wire basket*.

We can think of each of these sets in terms of an equivalence class of finite element nodes. The class of a node $x \in \Gamma$ is determined by the set of subdomains with x in their closures. We note that, for subdomains obtained from a mesh partitioner, the situation can be complicated and greater care with the definitions may be required; see, e.g., [28, section 3] and [27].

All elements of the coarse space are discrete saddle-point harmonic functions, in the sense of Definition 3.1, and are therefore determined solely by their values on the interface and are of minimal elastic energy.

In the plane, we introduce an edge cutoff function $\theta_{\mathcal{E}^{ij}}$ for each edge. It is a finite element function which equals 1 at all nodes of $\mathcal{E}^{ij}$ and vanishes at all other interface nodes. They are complemented by vertex cutoff functions $\theta_{\mathcal{V}^{i\ell}}$ which equal 1 at the vertex and vanish at all other interface nodes. Together these functions form a partition of unity. For $n = 2$, we then obtain all the elements in our coarse space by using these functions and the rigid body modes

$$\mathbf{r}_1 := \left[\begin{array}{c} 1 \\ 0 \end{array} \right], \quad \mathbf{r}_2 := \left[\begin{array}{c} 0 \\ 1 \end{array} \right], \quad \mathbf{r}_3 := \frac{1}{H_i} \left[\begin{array}{c} -x_2 + \hat{x}_2 \\ x_1 - \hat{x}_1 \end{array} \right].$$

Here $\hat{x}$ is a suitable shift, e.g., to the middle of the edge, to make this basis well conditioned. The scaling $1/H_i$ ensures that the norms of the three functions are comparable.

The basis functions of our coarse space are obtained by multiplying these vector valued functions by $\theta_{\mathcal{E}^{ij}}$ and bringing them into the finite element space by interpolating using the values at the nodes on the interface. We can obtain the same basis elements by restricting the three rigid body modes to the nodes of the edge and setting the values at all other interface nodes to zero. For each edge, we thus obtain three basis functions. In addition, we have two degrees of freedom for each vertex $\mathcal{V}^{i\ell}$ representing its displacement.

A similar construction is used for the three-dimensional case. The rigid body modes are now three translations

$$(4.1) \qquad \mathbf{r}_1 := \begin{bmatrix} 1 \\ 0 \\ 0 \end{bmatrix}, \quad \mathbf{r}_2 := \begin{bmatrix} 0 \\ 1 \\ 0 \end{bmatrix}, \quad \mathbf{r}_3 := \begin{bmatrix} 0 \\ 0 \\ 1 \end{bmatrix}$$

and three rotations

$$(4.2) \quad \mathbf{r}_4 := \frac{1}{H_i} \begin{bmatrix} 0 \\ -x_3 + \hat{x}_3 \\ x_2 - \hat{x}_2 \end{bmatrix}, \mathbf{r}_5 := \frac{1}{H_i} \begin{bmatrix} x_3 - \hat{x}_3 \\ 0 \\ -x_1 + \hat{x}_1 \end{bmatrix}, \mathbf{r}_6 := \frac{1}{H_i} \begin{bmatrix} -x_2 + \hat{x}_2 \\ x_1 - \hat{x}_1 \\ 0 \end{bmatrix},$$

where $\hat{x} \in \Omega_i$ can be chosen as a midpoint of an edge or face. The shift of the origin makes this basis for the space of rigid body modes well conditioned, and the scaling and shift make these six functions scale similarly with H_i.

For each face, we can use the products of a cutoff function $\theta_{\mathcal{F}^{ij}}$ with the rigid body modes or we can obtain six linearly independent basis functions by restricting the rigid body modes to the nodes of $\mathcal{F}^{ij}$ and setting the values at all other interface nodes to zero. For a straight edge, on the other hand, we obtain only five, since, as it is easy to see, a rigid body mode representing a rotation with the edge as its axis is invisible on the edge; for a detailed discussion of the case of curved edges, see [27] and also section 6. For each vertex, finally, we have three degrees of freedom representing the displacement at that point.

It is clear from our construction that when restricted to an interior subdomain, this coarse space will contain all the rigid body modes. As previously noted, this is a requirement for obtaining a scalable algorithm; see also [35, section 8.2].

As previously indicated, the local components of the preconditioner are based on a set of overlapping subdomains $\{\Omega_i'\}$. Each of them is associated with a bilinear form $\widetilde{a}_i'(\cdot, \cdot)$ obtained by integrating only over Ω_i' in (2.2) and then eliminating the pressure variables; i.e., this bilinear form corresponds to the displacement-only formulation. For the local problems, we use zero Dirichlet data on $\partial\Omega_i'$. Thus, our local spaces $\mathbf{V}_i', i = 1, \ldots, N$, are defined as

$$(4.3) \qquad \mathbf{V}_i' = \mathbf{V}^h(\Omega_i') \cap \mathbf{H}_0^1(\Omega_i').$$

This is the standard choice as in [35, Chapter 3].

All that is now required for the analysis of our algorithm is an estimate of a parameter in a stable decomposition of any element in the finite element space; see [35, Assumption 2.2 and Lemma 2.5]. We need to estimate C_0^2 in

$$(4.4) \qquad \widetilde{a}(\mathbf{u}_0, \mathbf{u}_0) + \sum_{i=1}^{N} \widetilde{a}_i'(\mathbf{u}_i, \mathbf{u}_i) \leq C_0^2 \widetilde{a}(\mathbf{u}, \mathbf{u}) \quad \forall \mathbf{u} \in \mathbf{V}^h$$

for some choice of $\{\mathbf{u}_i\}_0^N$ such that

(4.5)
$$\mathbf{u} = \sum_{i=0}^{N} R_i^T \mathbf{u}_i, \quad \mathbf{u}_i \in \mathbf{V}_i'.$$

Here $\widetilde{a}(\cdot, \cdot)$ is the displacement-only bilinear form for the entire domain Ω. For $i \geq 1$, we use the extension operators $R_i^T : \mathbf{V}_i' \longrightarrow \mathbf{V}^h$. Similarly, R_0^T imbeds $\mathbf{V}_0$ into $\mathbf{V}^h$.

Associated with the coarse space is a projection $P_0 : \mathbf{V}^h \longrightarrow \mathbf{V}_0$; it is orthogonal with respect to the $\widetilde{a}(\cdot, \cdot)-$inner product. For each local space $\mathbf{V}_i'$, there is a projection P_i defined by

$$P_i = R_i^T \widetilde{P}_i \quad \text{with} \quad \widetilde{P}_i \quad \text{defined by} \quad \widetilde{a}_i'(\widetilde{P}_i \mathbf{u}, \mathbf{v}) = \widetilde{a}(\mathbf{u}, R_i^T \mathbf{v}) \quad \forall \mathbf{v} \in \mathbf{V}_i'.$$

The additive Schwarz operator, the preconditioned operator used in our iteration, is given by

$$P_{ad} = \sum_{i=0}^{N} P_i.$$

By using [35, Lemmas 2.5 and 2.10], we find that the condition number $\kappa(P_{ad})$ can be bounded by $(N^C + 1)C_0^2$, where N^C is the minimal number of colors required to color the subdomains Ω_i' such that no pair of intersecting subdomains have the same color.

Our main result is as follows.

THEOREM 4.1 (condition number estimate). *The condition number of our domain decomposition algorithm satisfies*

$$\kappa(P_{ad}) \leq C(H/\delta)^3(1 + \log(H/\delta))(1 + \log(H/h)),$$

where C is a constant, independent of the number of subdomains and their diameters and the mesh size and which depends only on the number of colors required for the overlapping subdomains and the shape regularity of the elements and the subdomains.

As in many domain decomposition results, H/h is shorthand for $\max_i(H_i/h_i)$, where h_i is the smallest diameter of the elements of Ω_i. Similarly, H/δ is the largest ratio of H_i and δ_i. In our proof, we will assume that $\delta_i/h_i \leq C(H_i/\delta_i)$.

By using [35, Theorem 2.9], we can obtain a similar result for multiplicative Schwarz methods.

We note that the analysis of the compressible case would require only the use of older techniques as in [15]. The condition number can then be improved to

$$C(H/\delta)(1 + \log(H/h)).$$

See also [35, Chapter 8] for a survey of older results on domain decomposition algorithms for compressible elasticity.

5. Proof of main result. Our proof, which we now outline, is in three parts. As just indicated, we need to estimate the parameter C_0^2 of (4.4). To do so, we first design a coarse component $\mathbf{u}_0$ and provide a bound on $\widetilde{a}(\mathbf{u}_0, \mathbf{u}_0)$ by estimating $\widetilde{a}_i(\mathbf{u} - \mathbf{u}_0, \mathbf{u} - \mathbf{u}_0)$. The coarse interpolant $\mathbf{u}_0$ will be chosen so that we can estimate $\widetilde{a}_i(\mathbf{u} - \mathbf{u}_0, \mathbf{u} - \mathbf{u}_0)$ in terms of $a_i(\mathbf{u} - \mathbf{u}_0, \mathbf{u} - \mathbf{u}_0)$, by using Lemma 3.3, with a constant that does not grow with the parameter λ_i. In subsection 5.3, we will similarly design

and estimate the local components $\mathbf{u}_i$ of a partition of $\mathbf{u}$ as in (4.5), and we will again obtain a result which holds uniformly with respect to λ_i.

We can rely on some standard technical tools collected in [35, section 4.6] and [28, section 7]; they were developed for scalar elliptic problems and compressible elasticity, respectively. Thus, we can obtain estimates, in the norm defined by $a_i(\cdot,\cdot)$ in section 2 and by the matrix A of section 3, by using estimates in the $\mathbf{H}^1(\Omega_i)$-norm and the elementary inequality

$$(5.1) \qquad a_i(\mathbf{v},\mathbf{v}) = 2\int_{\Omega_i} \varepsilon(\mathbf{v}) : \varepsilon(\mathbf{v})dx \leq 2|\mathbf{v}|^2_{\mathbf{H}^1(\Omega_i)}.$$

We can then return to the norm defined by $a_i(\cdot,\cdot)$ by using the second Korn inequality.

LEMMA 5.1 (Korn's second inequality). *Let Ω_i be a Lipschitz domain of diameter H_i. Then, there exists a constant $C = C(\Omega_i)$ such that*

$$\|\mathbf{v}\|^2_{\mathbf{H}^1(\Omega_i)} \leq C\left(a_i(\mathbf{v},\mathbf{v}) + \frac{1}{H_i^2}\|\mathbf{v}\|^2_{\mathbf{L}^2(\Omega_i)}\right).$$

The norm of the left-hand side is the scaled $\mathbf{H}^1$-norm:

$$\|\mathbf{v}\|^2_{\mathbf{H}^1(\Omega_i)} := |\mathbf{v}|^2_{\mathbf{H}^1(\Omega_i)} + \frac{1}{H_i^2}\|\mathbf{v}\|^2_{\mathbf{L}^2(\Omega_i)}.$$

We note that the constant C in Lemma 5.1 depends on the shape regularity of the subdomain but that we will only need this result for the subdomains Ω_i, which, by assumption, are shape regular. In subsections 5.2 and 5.3, we will face other issues concerning domains with poor aspect ratios when we consider the inf-sup parameter, and other bounds which also depend on the aspect ratio will be part of the proof of our main result. We also note that inf-sup stability and Korn's second inequality are closely related; see, e.g., Bramble [7] in which new proofs of both results are given for general Lipschitz domains.

By using Lemma 5.1 and a Poincaré inequality, we obtain the following.

LEMMA 5.2. *Let Ω_i be a Lipschitz domain of diameter H_i. Then, there exists a constant $C = C(\Omega_i)$ such that*

$$\inf_{\mathbf{r}\in\mathcal{RB}} \|\mathbf{v} - \mathbf{r}\|^2_{\mathbf{H}^1(\Omega_i)} \leq Ca_i(\mathbf{v},\mathbf{v}).$$

Here $\mathcal{RB}$ is the space of rigid body modes.

A detailed discussion of variants of this result is given in [28, section 6]; in particular, Lemma 5.2 is closely related to [28, Lemma 6.4].

In a final, elementary step of our proof, we will use that $\mu_i a_i(\mathbf{v},\mathbf{v}) \leq \widetilde{a}_i(\mathbf{v},\mathbf{v})$.

We recall that $\mathbf{u}_0$ and indeed all elements of the coarse space are discrete saddle-point harmonic functions. Therefore, $\widetilde{a}(\mathbf{u}_0,\mathbf{u}_0) \leq \widetilde{a}(\mathbf{v},\mathbf{v})$ for any $\mathbf{v}$ which equals $\mathbf{u}_0$ on the interface Γ. Therefore, in the different steps of our proof, we can work with any extension into the interior of the subdomains which is convenient for us. We will focus on the more difficult case of $n = 3$ since no additional ideas are required for the case of $n = 2$.

5.1. The coarse component of the decomposition. As in the theory for iterative substructuring algorithms (see [35, Chapters 4, 5, and 6]), the analysis can be carried out for one subdomain Ω_i at a time and variations in the values of the Lamé parameters between subdomains will therefore not enter our bounds.

We recall that the coarse space, restricted to an individual subdomain that does not touch $\partial\Omega$, will contain all rigid body modes and that we have constructed a basis for the coarse space in terms of these modes and cutoff functions associated with the faces, edges, and vertices of the subdomain Ω_i. When constructing the coarse space component $\mathbf{u}_0$, by a specific interpolation procedure, we will make sure that all rigid body modes are reproduced and also that the remainder $\mathbf{w} = \mathbf{u} - \mathbf{u}_0$ will have a zero net flux across all the faces of the interface. Our construction and estimates can be used both for interior subdomains and for those with a boundary that intersects $\partial\Omega$ since our interpolation procedure will reproduce zero Dirichlet boundary conditions on $\partial\Omega_i \cap \partial\Omega$.

The construction of $\mathbf{u}_0$ begins by setting $\mathbf{u}_0(\mathcal{V}^{i\ell}) = \mathbf{u}(\mathcal{V}^{i\ell})$ at all vertices of the subdomain.

Next, for each edge $\mathcal{E}^{j\ell} \subset \partial\Omega_i$, common to two faces $\mathcal{F}^{ij}$ and $\mathcal{F}^{i\ell}$, we select the coefficients for the edge basis elements to minimize the $\mathbf{L}^2(\mathcal{E}^{j\ell})$-norm of $\mathbf{u} - \mathbf{u}_0$. We note that since an edge component is obtained by restricting rigid body modes to the nodes of the edge and $\mathbf{u} - \mathbf{u}_0$ vanishes at the subdomain vertices, we can find this component of $\mathbf{u}_0$ by solving

$$(5.2) \qquad \inf_{\mathbf{r}\in\mathcal{RB}} \|I^h(\theta_{\mathcal{E}^{j\ell}}(\mathbf{u}-\mathbf{r}))\|_{\mathbf{L}^2(\mathcal{E}^{j\ell})}.$$

Here I^h is the interpolation operator that maps any continuous function into the finite element space $\mathbf{V}^h$. Thus,

$$(5.3) \qquad \|I^h(\theta_{\mathcal{E}^{j\ell}}(\mathbf{u}-\mathbf{u}_0))\|_{\mathbf{L}^2(\mathcal{E}^{j\ell})} \leq \|I^h(\theta_{\mathcal{E}^{j\ell}}(\mathbf{u}-\mathbf{r}))\|_{\mathbf{L}^2(\mathcal{E}^{j\ell})} \quad \forall\mathbf{r}\in\mathcal{RB}.$$

We can estimate the $\mathbf{H}^1(\Omega_i)$-seminorm of this edge contribution by its $\mathbf{L}^2(\mathcal{E}^{j\ell})$-norm by using [35, Lemma 4.19]

$$|I^h(\theta_{\mathcal{E}^{j\ell}}\mathbf{u})|^2_{\mathbf{H}^1(\Omega_i)} \leq C\|\mathbf{u}\|^2_{\mathbf{L}^2(\mathcal{E}^{j\ell})}.$$

The proof of this result uses the trivial extension of the values on the edge to the nodes interior to Ω_i. The square of this $\mathbf{L}^2(\mathcal{E}^{j\ell})$-norm can, at the expense of a factor $C(1+\log(H_i/h_i))$, be estimated by the square of the $\mathbf{H}^1(\Omega_i)$-norm of $\boldsymbol{u}$ by using [35, Lemma 4.16]

$$\|\mathbf{u}\|^2_{\mathbf{L}^2(\mathcal{E}^{j\ell})} \leq C(1+\log(H_i/h_i))\|\mathbf{u}\|^2_{\mathbf{H}^1(\Omega_i)}.$$

These two results are combined in [35, Corollary 4.20], which we will use several times. Using these results, we then find that

$$(5.4) \qquad |I^h(\theta_{\mathcal{E}^{j\ell}}(\boldsymbol{u}-\boldsymbol{u}_0))|^2_{\mathbf{H}^1(\Omega_i)} \leq \inf_{\mathbf{r}\in\mathcal{RB}} C\|I^h(\theta_{\mathcal{E}^{j\ell}}(\mathbf{u}-\mathbf{r}))\|^2_{\mathbf{L}^2(\mathcal{E}^{j\ell})}$$

$$\leq \inf_{\mathbf{r}\in\mathcal{RB}} C\|\mathbf{u}-\mathbf{r}\|^2_{\mathbf{L}^2(\mathcal{E}^{j\ell})} \leq C(1+\log(H/h)) \inf_{\mathbf{r}\in\mathcal{RB}} \|\mathbf{u}-\mathbf{r}\|^2_{\mathbf{H}^1(\Omega_i)}.$$

Finally, for each face $\mathcal{F}^{ij} \subset \partial\Omega_i$ we determine the coefficients for the face basis functions by solving a constrained minimization problem with a single linear constraint. We recall that the restriction of $\boldsymbol{u}_0$ to a face is of the form $I^h(\theta_{\mathcal{F}^{ij}}\boldsymbol{r})$, where $\boldsymbol{r}$ is a linear combination of the six rigid body modes. We find this $\boldsymbol{r}$ by solving

$$(5.5) \qquad \inf_{\mathbf{r}\in\mathcal{RB}} \|I^h(\theta_{\mathcal{F}^{ij}}(\mathbf{u}-\mathbf{r}))\|^2_{\mathbf{L}^2(\mathcal{F}^{ij})} \text{ subject to } \int_{\mathcal{F}^{ij}} (\mathbf{u}-\mathbf{u}_0)\cdot\mathbf{n}\,dA = 0.$$

This gives rise to a well conditioned linear system of algebraic equations. All the matrix elements of the leading minor of order 6 are of order H_i^2; they are inner products in $\mathbf{L}^2(\mathcal{F}^{ij})$ of rigid body modes which, by construction, are of order 1. The remaining column and row of the matrix, which expresses the constraint, also have elements of order H_i^2. Simple estimates of the elements of the right-hand side of the linear system, using Cauchy–Schwarz's inequality, and a simple computation show that each coefficient for the face basis functions for $\boldsymbol{u}_0$ can be estimated by $(C/H_i)\|\boldsymbol{u}\|_{\mathbf{L}^2(\mathcal{F}^{ij})}$.

By a small modification of the proof of [35, Lemma 4.25], using the fact that the rigid body modes $\mathbf{r}_k$, defined in (4.1) and (4.2), have components which are linear functions which are uniformly bounded with gradients bounded by C/H_i, we have

$$(5.6) \qquad |I^h(\theta_{\mathcal{F}^{ij}}\mathbf{r}_k)|^2_{\mathbf{H}^1(\Omega_i)} \ \leq \ C(1 + \log(H_i/h_i))H_i, \quad k = 1, \ldots, 6.$$

Therefore, for the solution $\mathbf{r}$ of the constrained minimization problem (5.5), we have

$$(5.7) \qquad |I^h(\theta_{\mathcal{F}^{ij}}\mathbf{r})|^2_{\mathbf{H}^1(\Omega_i)} \leq C/H_i(1 + \log(H_i/h_i))\|\mathbf{u}\|^2_{L^2(\mathcal{F}^{ij})}.$$

By using an elementary trace theorem (see [32, Theorem 1.2] or [35, Lemma 4.17]), combining the estimates for the edge and face terms, and using the fact that $\mathbf{u} - \mathbf{u}_0$ vanishes at the subdomain vertices, we can conclude that

$$(5.8) \qquad |\mathbf{u} - \mathbf{u}_0|^2_{\mathbf{H}^1(\Omega_i)} \leq C(1 + \log(H_i/h_i))\|\mathbf{u}\|^2_{\mathbf{H}^1(\Omega_i)}.$$

Our recipe for $\mathbf{u}_0$ will clearly reproduce any rigid body mode. We can therefore replace $\|\mathbf{u}\|^2_{\mathbf{H}^1(\Omega_i)}$ on the right-hand side of (5.8) by $\inf_{\mathbf{r}\in\mathcal{RB}} \|\mathbf{u} - \mathbf{r}\|^2_{\mathbf{H}^1(\Omega_i)}$ and then use Lemma 5.2 and replace the square of that seminorm by $a_i(\mathbf{u}, \mathbf{u})$.

We now consider $\widetilde{a}_i(\mathbf{u} - \mathbf{u}_0, \mathbf{u} - \mathbf{u}_0)$. Since, by construction, the net flux across $\partial\Omega_i$ of $\mathbf{u} - \mathbf{u}_0$ vanishes, we can use Lemma 3.3 and estimate this energy by

$$4 \left(1 + \frac{n/2}{\mu_i/\lambda_i + \beta^2}\right) \mu_i a_i(\mathbf{u} - \mathbf{u}_0, \mathbf{u} - \mathbf{u}_0).$$

This expression, in turn, can, by using (5.1), be estimated by

$$8 \left(1 + \frac{n/2}{\mu_i/\lambda_i + \beta^2}\right) \mu_i|\mathbf{u} - \mathbf{u}_0|^2_{\mathbf{H}^1(\Omega_i)}$$

and therefore, by using (5.8) and the argument that follows, also by

$$C(1 + \log(H_i/h_i))\mu_i a_i(\mathbf{u}, \mathbf{u}).$$

We can then return to the $\widetilde{a}_i$-norm by using the elementary inequality $\mu_i a_i(\mathbf{u}, \mathbf{u}) \leq \widetilde{a}_i(\mathbf{u}, \mathbf{u})$.

A bound

$$\widetilde{a}(\mathbf{u}_0, \mathbf{u}_0) \leq C(1 + \log(H/h))\widetilde{a}(\mathbf{u}, \mathbf{u})$$

now results by adding the contributions from all the subdomains.

5.2. The influence of aspect ratios on certain bounds. Before we turn to the analysis of the local terms, we will formulate a result on the effect of the aspect ratios of domains on the inf-sup parameter. We also give bounds for certain modified face cutoff functions $\vartheta^\delta_{\mathcal{F}ij}$ which are supported in the closure of the set

$$(5.9) \qquad \Xi_{ij} := (\Omega_i \cup \mathcal{F}^{ij} \cup \Omega_j) \cap (\Omega'_i \cap \Omega'_j).$$

In addition, for each edge $\mathcal{E}^{j\ell} \subset \partial\Omega_i$, common to two faces $\mathcal{F}^{ij}$ and $\mathcal{F}^{i\ell}$ of Ω_i, we will consider a modified edge cutoff function $\vartheta^\delta_{\mathcal{E}j\ell}$. It is supported in the closure of the set

$$(5.10) \qquad \Psi_{j\ell} := \bigcap_{m \in I_{j\ell}} \Omega'_m,$$

which is the intersection of the extensions Ω'_m of all subdomains Ω_m, which have the edge $\mathcal{E}^{j\ell}$ in common with Ω_i. Here the set of subdomain indices, denoted by $I_{j\ell}$, also includes i.

Bounds over these two sets of domains, which have aspect ratios of order H_i/δ_i, will affect the estimates of the $\mathbf{u}_i \in \mathbf{V}'_i$, $i \geq 1$, in the decomposition which results in our estimate of C_0^2, the parameter in (4.4). In contrast, as previously noted, these aspect ratios do not enter the bound of the coarse space component $\mathbf{u}_0$ since all estimates required in subsection 5.1 are for entire subdomains which, by assumption, are shape regular.

We first consider the inf-sup parameter. The effect of the aspect ratio has been considered in the literature, in particular, by Dobrowolski [13]. As in that paper, which concerns the continuous problem, we consider a domain Ω and an $\alpha \in \mathbb{R}^n$ with

$$1 = \alpha_1 \leq \alpha_i \leq \alpha_n, \quad 1 \leq i \leq n.$$

A stretched domain is then defined by

$$\Omega_\alpha = \{y \in \mathbb{R}^n : (y_1/\alpha_1, \ldots, y_n/\alpha_n) \in \Omega\}.$$

Additional geometric parameters d_i, the diameters of Ω with respect to the coordinate directions, are defined by

$$d_i = \sup\{h : x, x + he_i \in \Omega\}, \quad 1 \leq i \leq n.$$

For our application, the lower bound of the following result will provide a bound on β, which decreases no faster than linearly in δ/H for the domains defined by (5.9) and (5.10).

LEMMA 5.3 (Dobrowolski). *The* inf-sup *parameter* $\beta(\Omega_\alpha)$ *of the stretched domain satisfies*

$$\frac{\beta(\Omega)}{\alpha_n} \leq \beta(\Omega_\alpha) \leq \frac{C}{\alpha_n},$$

where $C^2 = d_1^3 d_2 \ldots d_n/d^{n+2}$ *and* d *is the length of the side of the largest n-cube that is contained in* Ω.

To obtain the same result as in Lemma 5.3, for the discrete case, we combine this lemma with techniques developed in Stenberg [34]. We note that his arguments are in terms of macroelements; i.e., local arguments are sufficient. Therefore, the aspect ratio of the domain enters only through the inf-sup parameter for the continuous problem.

A standard tool in the theory for iterative substructuring problems is provided by [35, Lemma 4.24]

$$(5.11) \qquad |I^h(\vartheta_{\mathcal{F}^{ij}}\mathbf{u})|^2_{\mathbf{H}^1(\Omega_i)} \le C(1 + \log(H_i/h_i))^2 \|\mathbf{u}\|^2_{\mathbf{H}^1(\Omega_i)}.$$

Here $\vartheta_{\mathcal{F}^{ij}}$ is an explicitly constructed function, which has the same boundary values as $\theta_{\mathcal{F}^{ij}}$ on Γ. We also have the bound

$$(5.12) \qquad |\vartheta_{\mathcal{F}^{ij}}|^2_{\mathbf{H}^1(\Omega_i)} \le C(1 + \log(H_i/h_i))H_i;$$

see [35, Lemma 4.25].

In our analysis of the local terms, we need similar bounds but for the intersection of Ω_i with Ω'_j, the extension of the other subdomain Ω_j, which has a face $\mathcal{F}^{ij}$ in common with Ω_i. We will use a face cutoff function $\vartheta^{\delta}_{\mathcal{F}^{ij}}$ which is different from $\vartheta_{\mathcal{F}^{ij}}$ in two respects. Instead of having the value 1 at all nodes of $\mathcal{F}^{ij}$, it will equal $dist(x, \partial\mathcal{F}^{ij})/\delta_i$, at any node $x \in \mathcal{F}^{ij}$ within a distance δ_i of the boundary of the face; at all other nodes on $\mathcal{F}^{ij}$ the nodal values remain 1. We note that this function thus resembles a regular face cutoff function on a coarser mesh with elements of size δ_i. In addition, we will restrict the support of this cutoff function to the closure of Ξ_{ij}. The bound on the right-hand side of (5.11) must then be multiplied by a factor H_i/δ_i. On the other hand, one of the factors $(1+\log(H_i/h_i))$ can be replaced by $(1+\log(H_i/\delta_i))$.

LEMMA 5.4. *There exists a face cutoff function $\vartheta^{\delta}_{\mathcal{F}^{ij}}$, with values at the nodes of $\mathcal{F}^{ij}$ as just specified, which vanishes at all the nodes on the rest of the boundary of $\Omega_i \cap \Omega'_j$ and which satisfies*

$$(5.13) \quad |I^h(\vartheta^{\delta}_{\mathcal{F}^{ij}}\mathbf{u})|^2_{\mathbf{H}^1(\Omega_i \cap \Omega'_j)} \le C(H_i/\delta_i)(1 + \log(H_i/\delta_i))(1 + \log(H_i/h_i))\|\mathbf{u}\|^2_{\mathbf{H}^1(\Omega_i)}$$

and for all the $\mathbf{r}_k$, the basis elements of the space $\mathcal{RB}$,

$$(5.14) \qquad |I^h(\vartheta^{\delta}_{\mathcal{F}^{ij}}\mathbf{r}_k)|^2_{\mathbf{H}^1(\Omega_i \cap \Omega'_j)} \le C(H_i/\delta_i)(1 + \log(H_i/\delta_i))H_i.$$

We will prove this result for a square face and for a cube compressed in the direction normal to $\mathcal{F}^{ij}$, i.e., a domain which has dimensions $H_i \times H_i \times \delta_i$. We note that the result also holds for any domain which contains this compressed cube and shares the face $\mathcal{F}^{ij}$ with it. Therefore, the boundary of the extended subdomains Ω'_j can be quite irregular; we simply extend $\vartheta^{\delta}_{\mathcal{F}^{ij}}$ by zero into the rest of Ω_i. The proof can also easily be modified to hold for other geometric configurations such as a neighborhood, of minimal thickness δ_i, of a face of a tetrahedron. As we will see, we need only a positive lower bound for the angles between the faces of Ω_i that meet at the edges of the face $\mathcal{F}^{ij}$. We will begin our proof by considering functions $\vartheta^H_{\mathcal{F}^{ij}}$ defined in the entire cube prior to its compression.

Proof. We first note that the presence of the interpolation operator I^h in our formulas present no difficulties; see [35, Lemma 4.31]. To establish (5.13), we need to examine and modify the proofs of [35, Lemmas 4.23, 4.24, and 4.25]. Those proofs concern four functions $\vartheta_{\mathcal{F}^{ij}}$, one for each face of a shape regular tetrahedron of diameter H.

An analogous construction for a cube is worked out in the doctoral thesis of Casarin [11, subsection 3.3.2] and will now be outlined. While, in the proof of [35, Lemma 4.23], the tetrahedral subdomain is divided into four tetrahedra by connecting its vertices to its centroid, the cube is divided into six pyramids each with a face of the cube as its base. Similar to the tetrahedral case, these pyramids are each divided

into four tetrahedra each with an edge selected from among the edges of the cube and another edge connecting the centroid of the cube with the centroid of a face of the cube that is adjacent to the first edge. The construction given below will show that a function $\vartheta^H_{\mathcal{F}^{ij}}$ can be constructed such that

$$(5.15) \quad |\nabla \vartheta^H_{\mathcal{F}^{ij}}(x)| \quad \leq \quad C/r \ \text{ for } \ r \geq \delta_i, \ \text{ and } \ |\nabla \vartheta^H_{\mathcal{F}^{ij}}(x)| \quad \leq \quad C/\delta_i \ \text{ for } \ r \leq \delta_i.$$

Here C is a constant and r the minimum distance of x to the wire basket of the cube.

Before we consider the effects of compressing the cube, we will provide some further details on the construction. For the cube, $\vartheta^H_{\mathcal{F}^{ij}}(x)$ is defined as follows: its values on the line segment between the centroid of the cube and the centroid of the face $\mathcal{F}^{ij}$ vary linearly from $1/6$ to 1. Similarly, the restriction of $\vartheta^H_{\mathcal{F}^{ij}}$ to the line segments between the centroid of the cube and the centroids of the other faces drops linearly from $1/6$ to 0. The value elsewhere in each of the 24 tetrahedra is given, for all points at a distance larger than δ_i from the wire basket, by a constant value on any plane through the edge of the cube, which intersects one of the line segments just introduced, with its value determined by that on the line segment. For the part on any such plane, which is within δ_i of the wire basket, we will let the function decrease linearly to zero as a function of the distance to the wire basket. The bounds on the gradient of the resulting function, as in (5.15), then follow easily. We also note that these modified face functions will give us a partition of unity for the whole cube with the exception of a δ_i-neighborhood of the wire basket. Clearly, this will no longer be true after we compress the support of the individual face functions.

We now examine the effect of compressing the cube in the direction normal to the face $\mathcal{F}^{ij}$ which results in the function $\vartheta^\delta_{\mathcal{F}^{ij}}$. With the new dimensions $H_i \times H_i \times \delta_i$ the gradient of $\vartheta^\delta_{\mathcal{F}^{ij}}$ can be estimated by $CH_i/r\delta_i$ in the interior of this domain and by CH_i/δ_i^2 in the image, under the compression, of the δ_i-neighborhood of the wire basket. These bounds are best possible for the four tetrahedra adjacent to the face $\mathcal{F}^{ij}$ and reflect the fact that the angle between two faces, of any subtetrahedron, which has an edge of the cube in common with and is adjacent to $\mathcal{F}^{ij}$, shrinks by a factor $\arctan(\delta_i/H_i)$. On the other hand, for the other tetrahedra adjacent to the edges of the face $\mathcal{F}^{ij}$, the angle in fact increases and the gradient decreases. In still others, the angles are also decreased, but there are no additional difficulties treating the neighborhood of the edges of the face opposite to $\mathcal{F}^{ij}$.

We also recall that the estimates of the energy of $I^h(\vartheta_{\mathcal{F}^{ij}}\mathbf{u})$, in the proof of [35, Lemma 4.24], involve the introduction of cylindrical coordinates with individual edges of $\partial\mathcal{F}^{ij}$ as z-axes and integrating over individual subtetrahedra. In fact, we integrate over the images of the δ_i-neighborhoods of the edges and the remaining parts of the subtetrahedra separately; the latter will contribute a $\log(H_i/\delta_i)$ factor. The linear factor H_i/δ_i in (5.13) results from the fact that while the square of the gradient of $\vartheta^\delta_{\mathcal{F}^{ij}}(x)$ grows quadratically in H_i/δ_i in the tetrahedra next to the face, the angle over which we integrate shrinks in proportion to δ_i/H_i. The bounds for the contributions to the norm by the other twenty subtetrahedra pose no additional difficulties.

As in [35, Proof of Lemma 4.24], we also use a bound on the L_2-norm of finite element functions over intervals of length H_i, which are parallel to edges of the cube; see [35, Corollary 4.20]. We can use that result without any concern for the aspect ratios of our regions after noting that the finite element function $\mathbf{u}$ is defined in all of Ω_i and writing our bound, as in the right-hand side of (5.13), in terms of the norm over the entire subdomain.

The arguments given above can easily be modified to establish the bound in (5.14). □

The modified edge function $\vartheta^\delta_{\mathcal{E}^{j\ell}}$ is supported in the closure of a δ_i-neighborhood of the wire basket of Ω_i and in the closure of $\Psi_{j\ell}$. We no longer have to work with the compressed cube. The $\vartheta^\delta_{\mathcal{E}^{j\ell}}$ of all the edges of Ω_i, the $\vartheta^\delta_{\mathcal{F}^{j\ell}}$ of all the faces of the subdomain, and the standard nodal basis functions of the subdomain vertices should form a partition of unity when restricted to $\partial\Omega_i$. It is straightforward to construct such an edge function which satisfies $|\nabla\vartheta^\delta_{\mathcal{E}^{j\ell}}| \leq C/\delta_i$ except in the elements next to the subdomain vertices; the effect of the resulting large gradients in these few elements will cause no difficulties. By introducing cylindrical coordinates, with the edge as the z-axis, and again using [35, Corollary 4.20], we can prove the following.

LEMMA 5.5. *There exists an edge cutoff function $\vartheta^\delta_{\mathcal{E}^{j\ell}}$ supported in the closure of $\Psi_{j\ell}$, which, together with the face cutoff function $\vartheta^\delta_{\mathcal{F}^{ik}}$ and the standard nodal basis functions of the subdomain vertices, forms a partition of unity on $\partial\Omega_i$ and which satisfies*

$$(5.16) \qquad |I^h(\vartheta^\delta_{\mathcal{E}^{j\ell}}\mathbf{u})|^2_{\mathbf{H}^1(\Psi_{j\ell})} \leq C(1 + \log(H_i/h_i))\|\mathbf{u}\|^2_{\mathbf{H}^1(\Omega_i)}$$

and for all the $\mathbf{r}_k$, the basis functions of the space $\mathcal{RB}$,

$$(5.17) \qquad |I^h(\vartheta^\delta_{\mathcal{E}^{j\ell}}\mathbf{r}_k)|^2_{\mathbf{H}^1(\Psi_{j\ell})} \leq CH_i.$$

In the next subsection, we will find that our bounds will be proportional to $(H/\delta)^3$ with two of the factors originating from the inf-sup parameter and Lemmas 3.3 and 5.3 and one from the bounds in (5.13) and (5.14).

5.3. The local components of the partitioning. The standard way of constructing and estimating the local components $\mathbf{u}_i \in \mathbf{V}'_i$, as in (4.4), involves a partition of unity for all $x \in \Omega$; see [35, sections 3.2 and 3.6]. Here we adopt a different strategy. We will again consider only the three-dimensional case.

We first remove the interior components of $\mathbf{w} = \mathbf{u} - \mathbf{u}_0$ for each subdomain; they vanish on the interface and are made $\tilde{a}_i$-orthogonal to the space of the discrete saddle-point harmonic functions defined in (3.17). Therefore, each of these interior functions can be bounded directly by the energy of $\mathbf{w}$ contributed by an individual subdomain, and they therefore contribute to the individual components $\mathbf{u}_i$ in a harmless way. To simplify our notation, we will now denote by $\mathbf{w}$ what remains after this correction.

We will now explore how the restriction $\mathbf{w}_i$ of $\mathbf{w}$ to Ω_i can be partitioned. For each face $\mathcal{F}^{ij}$, we will have contributions to $\mathbf{u}_i$ and $\mathbf{u}_j$, and for each edge $\mathcal{E}^{j\ell}$, there will be contributions to $\mathbf{u}_m \ \forall m \in I_{j\ell}$; cf. (5.10). In all that follows, we will look exclusively at the contributions from Ω_i. We also have to make sure that our constructions lead to terms which are continuous functions across the interface Γ between the subdomains.

We first decompose the restriction of $\mathbf{w}_i$ to Γ_i into face and edge terms by using the cutoff functions $\vartheta^\delta_{\mathcal{F}^{ij}}$ and $\vartheta^\delta_{\mathcal{E}^{i\ell}}$. We estimate the energy of $I^h(\vartheta^\delta_{\mathcal{F}^{ij}}\mathbf{u})$ and $I^h(\vartheta^\delta_{\mathcal{F}^{ij}}\mathbf{u}_0)$ separately. For the first term, we can use (5.13) directly. To get a bound of the same quality for the second term, we return to the arguments that led to (5.7). We use the same bound for the coefficient of the coarse face basis functions of the solution of the constrained minimization problem $(C/H_i)\|\mathbf{u}\|_{\mathbf{L}^2(\mathcal{F}^{ij})}$ and replace (5.6) by (5.14). We find that

$$|I^h(\vartheta^\delta_{\mathcal{F}^{ij}}\mathbf{w}_i)|^2_{\mathbf{H}^1(\Omega_i \cap \Omega'_j)} \leq C(H_i/\delta_i)(1 + \log(H_i/\delta_i))(1 + \log(H_i/h_i))\|\mathbf{u}\|^2_{\mathbf{H}^1(\Omega_i)}.$$

We can replace $\|\mathbf{u}\|^2_{\mathbf{H}^1(\Omega_i)}$ by $\inf_{\mathbf{r}\in\mathcal{RB}}\|\mathbf{u} - \mathbf{r}\|^2_{\mathbf{H}^1(\Omega_i)}$ by using that the interpolant, which gives us $\mathbf{u}_0$, reproduces any rigid body mode.

Similarly, we can use Lemma 5.5 to estimate the norm of $I^h(\vartheta^\delta_{\mathcal{E}^{j\ell}}\mathbf{u})$. To estimate the norm of $I^h(\vartheta^\delta_{\mathcal{E}^{j\ell}}\mathbf{u}_0)$, we partition $\mathbf{u}_0$ by using $\theta_{\mathcal{F}^{ij}}$, $\theta_{\mathcal{F}^{i\ell}}$, and $\theta_{\mathcal{E}^{j\ell}}$. The first term $I^h(\theta_{\mathcal{F}^{ij}}\vartheta^\delta_{\mathcal{E}^{j\ell}}\mathbf{u}_0)$ can be estimated by again examining the arguments that led to (5.7) now using (5.17) instead of (5.6). The second face term can be estimated in exactly the same way. As for the contribution from the values on the edge $\mathcal{E}^{j\ell}$, we can estimate $I^h(\theta_{\mathcal{E}^{j\ell}}\vartheta^\delta_{\mathcal{E}^{j\ell}}\mathbf{w}_i)$ directly by using (5.4). This is possible since, on $\partial\Omega_i$, $\theta_{\mathcal{E}^{j\ell}}\vartheta^\delta_{\mathcal{E}^{j\ell}}$ vanishes except at the nodes of the edge, and we can use a trivial extension to the interior of Ω_i in our estimate. Thus, we obtain

$$|I^h(\vartheta^\delta_{\mathcal{E}^{j\ell}}\mathbf{w})|^2_{\mathbf{H}^1(\Omega_i)} \le C(1 + \log(H_i/h_i)) \inf_{\mathbf{r}\in\mathcal{RB}} \|\mathbf{u} - \mathbf{r}\|^2_{\mathbf{H}^1(\Omega_i)}.$$

We recall that, by construction, the net flux of $\mathbf{w} = \mathbf{u} - \mathbf{u}_0$, across each face of the subdomain, vanishes. However, this will generally no longer be true for $I^h(\vartheta^\delta_{\mathcal{F}^{ij}}\mathbf{w}_i)$ and $I^h(\vartheta^\delta_{\mathcal{E}^{j\ell}}\mathbf{w}_i)$. We will therefore modify these face and edge contributions to ensure that the net fluxes of the modified face and edge functions will vanish separately. This then makes it possible to use Lemma 3.3.

For each face $\mathcal{F}^{ij}$ and for each edge $\mathcal{E}^{j\ell}$ of that face, we select a subset $\widehat{\mathcal{F}}^{ij\ell}$, of the face $\mathcal{F}^{ij}$, which belongs to the intersection $\Xi_{ij} \cap \Psi_{j\ell}$ and which does not intersect the sets Ψ_{km} which are neighborhoods of the other edges of Ω_i. This subset should have an area on the order of $H_i\delta_i$, and we should be able to cover it by on the order of H_i/δ_i square patches with side δ_i. We will find, and later estimate, a parameter $d_{ij\ell}$ so that

$$(5.18) \qquad\qquad I^h(\vartheta^\delta_{\mathcal{E}^{j\ell}}\mathbf{w}_i) - d_{ij\ell}\vartheta_{\widehat{\mathcal{F}}^{ij\ell}}\mathbf{n}_{ij}$$

has a zero net flux across the face $\mathcal{F}^{ij}$. Here $\vartheta_{\widehat{\mathcal{F}}^{ij\ell}}$ is a sum of on the order of H_i/δ_i face functions for cubes of side δ_i, and $\mathbf{n}_{ij}$ is the normal to the face $\mathcal{F}^{ij}$.

The face contributions are then modified by adding these correction terms, one for each of the edges of the face, resulting in a face function $\mathbf{w}_{\mathcal{F}^{ij}}$ with a zero net flux across $\mathcal{F}^{ij}$. The modified face contribution is defined by

$$(5.19) \qquad\qquad \mathbf{w}_{\mathcal{F}^{ij}} := I^h(\vartheta^\delta_{\mathcal{F}^{ij}}\mathbf{w}_i) + \sum_k d_{ijk}\vartheta_{\widehat{\mathcal{F}}^{ijk}}\mathbf{n}_{ij}.$$

Similarly, the modified edge contribution for $\mathcal{E}^{j\ell}$ is defined by

$$(5.20) \qquad\qquad \mathbf{w}_{\mathcal{E}^{j\ell}} := I^h(\vartheta^\delta_{\mathcal{E}^{j\ell}}\mathbf{w}) - d_{ij\ell}\vartheta_{\widehat{\mathcal{F}}^{ij\ell}}\mathbf{n}_{ij} - d_{i\ell j}\vartheta_{\widehat{\mathcal{F}}^{i\ell j}}\mathbf{n}_{i\ell}.$$

We note that the third term represents a displacement in the direction normal to the second face $\mathcal{F}^{i\ell}$ of Ω_i, which is also adjacent to the edge $\mathcal{E}^{j\ell}$, and that the second coefficient $d_{i\ell j}$ is chosen so that there is a zero net flux across that face.

It remains to find bounds for the individual face corrections. We need to estimate the energy of $\vartheta_{\widehat{\mathcal{F}}^{ij\ell}}$ as well as the parameter $d_{ij\ell}$. Since $\vartheta_{\widehat{\mathcal{F}}^{ij\ell}}$ is a sum of on the order of H_i/δ_i face functions for cubes of side δ_i, we can use the estimate (5.12) after replacing H_i by δ_i. Therefore,

$$|\vartheta_{\widehat{\mathcal{F}}^{ij\ell}}|^2_{\mathbf{H}^1(\Omega_i\cap\Omega'_j)} \le C(H_i/\delta_i)(1 + \log(\delta_i/h_i))\delta_i.$$

The parameter $d_{i\ell}$ is determined by the zero net flux condition for the modified edge term (5.18). By using Cauchy–Schwarz's inequality, we find that

$$|d_{ij\ell}|^2 \le C/(H_i\delta_i)\|\mathbf{w}_i\|^2_{L^2(\widehat{\mathcal{F}}^{ij\ell})}.$$

By using a trace theorem, essentially as in the proof of (5.8), and that same inequality, we can estimate this face correction term by

$$C(H_i/\delta_i)(1 + \log(\delta_i/h_i))\|\mathbf{w}_i\|^2_{\mathbf{H}^1(\Omega_i)} \le$$
$$C(H_i/\delta_i)(1 + \log(\delta_i/h_i)) \inf_{\mathbf{r}\in\mathcal{RB}}\|\mathbf{u} - \mathbf{r}\|^2_{\mathbf{H}^1(\Omega_i)}.$$

These bounds are all consistent with Theorem 4.1.

We now show how to divide $\mathbf{w}_{\mathcal{F}^{ij}}$, given in (5.19), into contributions to $\mathbf{u}_i$ and $\mathbf{u}_j$, which are the contributions of $\mathbf{V}'_i$ and $\mathbf{V}'_j$, respectively, to the decomposition (4.5). We allocate $(1/2)\mathbf{w}_{\mathcal{F}^{ij}}$ to $\mathbf{u}_j$, and, to start constructing $\mathbf{u}_i$, we subtract the same function from $\mathbf{w}_i$. With the same recipe used for Ω_j, the subdomain across the face $\mathcal{F}^{ij}$, we see that these contributions to $\mathbf{u}_i$ and $\mathbf{u}_j$ will be continuous. Each of them also has a zero net flux across $\partial\Omega_i$.

We then partition the edge function $\mathbf{w}_{\mathcal{E}^{j\ell}}$ given in (5.20). If p subdomains share the edge, we then divide this function by p and add it to the contributions from the faces to $\mathbf{u}_m, m \ne i, m \in I_{i\ell}$. To obtain $\mathbf{u}_i$, we subtract these $p - 1$ contributions from the function previously obtained from $\mathbf{w}_i$ by subtracting $(1/2)\mathbf{w}_{\mathcal{F}^{ij}}$ for each face of Ω_i. We note that all the resulting $\mathbf{u}_m$ will, by construction, satisfy the no net flux condition and that we maintain continuity across the interface.

By using the no net flux condition, Lemmas 5.3 and 3.3, and that the aspect ratios of $\Omega_i \cap \Omega'_k$ are on the order of H_i/δ_i, we find that

$$\widetilde{a}_i(\mathbf{u}_m, \mathbf{u}_m) \le C(H_i/\delta_i)^2\mu_i a_i(\mathbf{u}_m, \mathbf{u}_m).$$

Therefore, any of the contributions to $\mathbf{u}_m$ from an edge of Ω_i can be estimated by

$$C(H_i/\delta_i)^3(1 + \log(\delta_i/h_i))(1 + \log(H_i/h_i))\widetilde{a}_i(\mathbf{u}, \mathbf{u}).$$

Similarly, each of the face contributions can be estimated with a factor

$$C(H_i/\delta_i)^3(1 + \log(H_i/\delta_i))(1 + \log(H_i/h_i)).$$

This completes the proof of Theorem 4.1.

6. The effect of irregular subdomain boundaries. As we have seen, the assumption that the subdomains are quite regular (cf. subsection 2.2) makes it possible to use many technical tools, which have been used previously in many studies. This represented the state of the art of domain decomposition theory as of a couple of years ago. Thus, the same [35, Assumption 4.3] was used when obtaining many results on iterative substructuring algorithms given in Chapters 4–6 in that monograph. However, subdomains are often generated by mesh partitioners such as METIS [23], and, in practice, there is no guarantee that the subdomains are even uniformly Lipschitz continuous. We also note that if we change the mesh size of our problem and use the mesh partitioner again, we must expect that the new subdomains will not be related in any meaningful way to those obtained for the previous mesh; e.g., their number may very well have changed.

Recently, there has been considerable progress in developing new techniques, which require very limited regularity of the subdomain boundaries and with bounds which depend only on a few geometric parameters, which are easy to understand; see [15, 26]. These papers concern problems in the plane. We will find that our results in this paper can be extended to the same more general class of subdomains for the case

of two dimensions. We will also explore the three-dimensional case. We note that the regularity of $\partial\Omega$, the boundary of the given domain, will play no role.

The minimal assumption used in our recent papers is that the subdomains are John domains.

DEFINITION 6.1 (John domain). *A domain $\Omega \subset \mathbb{R}^n$—an open, bounded, and connected set—is a John domain if there exist a constant $C_J \geq 1$ and a distinguished central point $x_0 \in \Omega$ such that each $x \in \Omega$ can be joined to it by a rectifiable curve $\gamma : [0,1] \to \Omega$ with $\gamma(0) = x_0$, $\gamma(1) = x$, and $|x - \gamma(t)| \leq C_J \cdot distance(\gamma(t), \partial\Omega)$ for all $t \in [0,1]$.*

This condition can be viewed as a twisted cone condition. We note that certain Koch snowflake curves with fractal boundaries are John domains. We note that the parameter C_J will depend on the aspect ratio as well as the boundary of the domain.

In many domain decomposition studies, an extension theorem is also required; see, e.g., [26]. An important extension theorem was established in [22] for all *uniform* domains. A uniform domain satisfies the John condition and can also have quite an irregular boundary such as that of a Koch snowflake.

An important tool in the theory on domain decomposition algorithms is Poincaré's inequality; see [15].

LEMMA 6.2 (Poincaré's inequality). *Let Ω be a John domain. Then, with $\bar{u}_\Omega$ the average of u over Ω,*

$$\|u - \bar{u}_\Omega\|_{L_2(\Omega)}^2 \leq (\gamma(\Omega, n))^2 |\Omega|^{2/n} \|\nabla u\|_{L_2(\Omega)}^2 \quad \forall u \in H^1(\Omega).$$

Here the parameter $\gamma(\Omega, n)$ is the best parameter in an isoperimetric inequality

$$(6.1) \qquad [\min(|A|, |B|)]^{1-1/n} \leq \gamma(\Omega, n)|\partial A \cap \partial B|.$$

Here $A \subset \Omega$ is an arbitrary open set $B = \Omega \setminus \bar{A}$ and $|A|$ is the measure of the set A, etc.

We note that it is known that any simply connected plane domain, with a finite parameter $\gamma(\Omega, 2)$, is a John domain; see [10]. It is also known (see [6]) that any John domain has a bounded parameter $\gamma(\Omega, n)$.

In the present paper, the role of the Poincaré inequality is played by Lemma 5.2. This result has been established for uniform domains in [19], and a closely related result is given in [1] for John domains. Following [8, Lemma 11.2.3], we note that the inf-sup constant β, for the continuous problem, is the best constant in the estimate

$$\beta\|\mathbf{u}\|_{H^1(\Omega)} \leq \|p\|_{L_2(\Omega)},$$

where $\mathbf{u}$ is a solution of div $\mathbf{u} = p$ in $\mathbf{H}_0^1(\Omega)$. This inequality has been established for John domains in [1]. The parameter β depends only on the John parameter C_J.

A bound similar to (5.8) can be established for John domains in two dimensions. The factor of $(1 + \log(H/h))$, which will weaken our main result, should replace $(1 + \log(H/\delta))$. This is similar to what happens in the proof of [15, Theorem 3.1], and for the same reason—a standard trace theorem is missing for general John domains and in our proof—a bound on the L^∞-norm of finite element functions is used; see [15, Lemma 3.2] for a proof for two-dimensional John domains. Estimates for edge cutoff functions, very similar to those for faces in this paper, are also known; see [26, Lemma 4.4]. By examining the rest of our proof in section 5, we find that the slightly weaker form of the main result of this paper will hold for the case of John subdomains in two dimensions.

For problems in three dimensions, the set of tools is still much less complete. One reason is that the John and uniform conditions then do not rule out that part of a middle of a face is very close to another face. This is unlikely to be a real issue in our application since, in subsections 5.2 and 5.3, we work with domains which, by assumption, have a minimal thickness δ_i. Currently, a main open problem is to extend the bound in (5.11) under some appropriate geometric assumptions, which would be realistic for subdomains such as those generated by mesh partitioners.

7. Numerical examples. Numerical examples are presented in this section for unit square domains in two dimensions and unit cube domains in three dimensions. Homogeneous Dirichlet conditions are applied to the entire boundary in both cases. We consider both structured and unstructured mesh decompositions. For the structured decompositions, the subdomains are squares in two dimensions and cubes in three dimensions. For the unstructured decompositions, the graph partitioning software METIS [23] was used to decompose the mesh into N subdomains. Two examples of unstructured mesh decompositions are shown in Figure 7.1. All the examples used preconditioned conjugate gradients to solve the preconditioned linear system corresponding to the Schwarz operator P_{ad} to a relative residual tolerance of 10^{-8} for random right-hand sides. Numbers of iterations (iter) and condition number estimates (cond), from the conjugate gradient iterations, are reported in each of the following tables.

7.1. Two dimensions. Results for fixed values of $H/h = 8$ and $H/\delta = 4$ are shown in Table 7.1 for increasing numbers of subdomains N and three different values of Poisson ratio ν. As expected, condition number estimates appear to be bounded independently of both N and ν in the case of structured decompositions. We note that the same number of layers of additional elements were used for the overlapping subdomains for both types of mesh decompositions. Good scalability is also evident for unstructured decompositions, but there is more variability in the results. We note in the final row of Table 7.1 that the mesh was originally decomposed into 256 subdomains, but two of these subdomains had disconnected components which led to a total of 258 subdomains. Ideally, each subdomain would have 64 elements, but one
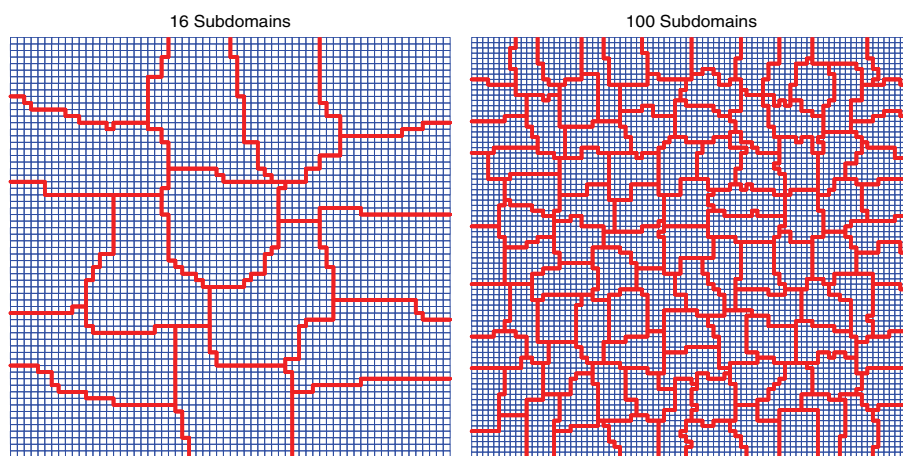

FIG. 7.1. *Examples of unstructured mesh decompositions used in numerical examples.*

TABLE 7.1
Two-dimensional results for $H/h = 8$, $H/\delta = 4$, and increasing numbers of subdomains N.

N	structured decomposition						unstructured decomposition					
	$\nu = 0.3$		$\nu = 0.4999$		$\nu = 0.49999$		$\nu = 0.3$		$\nu = 0.4999$		$\nu = 0.49999$	
	iter	cond	iter	cond	iter	cond	iter	cond	iter	cond	iter	cond
16	25	8.1	31	10.6	33	10.6	28	8.0	34	12.2	36	12.3
36	27	8.6	32	11.0	33	11.0	34	11.6	41	18.8	42	18.7
64	29	8.9	32	11.2	34	11.2	34	11.0	42	18.9	43	19.0
100	30	9.2	32	11.2	35	11.2	34	10.9	39	16.7	40	16.7
256*	32	9.7	34	11.6	35	11.7	38	12.6	44	23.1	45	23.1

TABLE 7.2
Two-dimensional results for $N = 16$, $H/\delta = 4$, and increasing values of H/h.

H/h	structured decomposition						unstructured decomposition					
	$\nu = 0.3$		$\nu = 0.4999$		$\nu = 0.49999$		$\nu = 0.3$		$\nu = 0.4999$		$\nu = 0.49999$	
	iter	cond	iter	cond	iter	cond	iter	cond	iter	cond	iter	cond
8	25	8.05	31	10.6	33	10.6	29	8.71	34	14.3	34	14.3
16	27	8.89	33	12.3	34	12.3	33	11.4	40	18.1	41	18.2
32	28	9.67	35	14.1	36	14.1	29	8.18	34	12.8	34	12.8
64	30	10.4	36	15.8	38	15.8	33	9.89	38	16.0	40	16.1
128	31	11.0	38	17.4	40	17.4	33	9.76	40	18.1	41	18.1

of the subdomains had only 5 elements. Fortunately, the numerical results do not appear to be greatly sensitive to such imbalances.
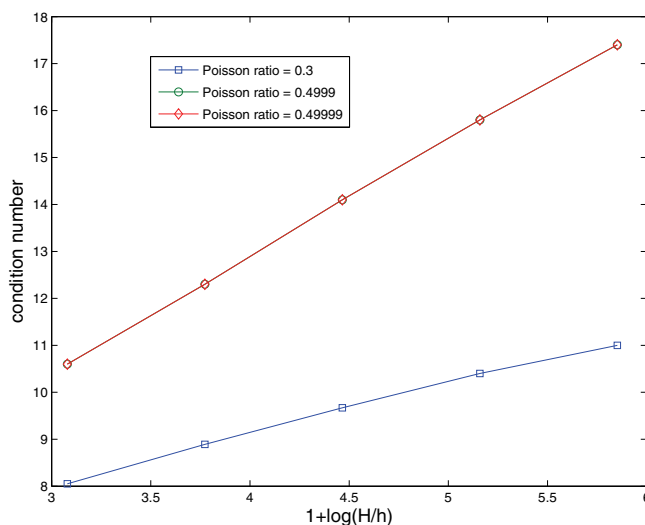

FIG. 7.2. *Two-dimensional results from Table* 7.2.

The next example investigates the effect of increasing H/h while fixing $N = 16$ and $H/\delta = 4$. The results on the left side of Table 7.2 are also plotted in Figure 7.2. Notice that condition number estimates appear to be bounded by a constant times $1 + \log(H/h)$ for all values of ν. This bound is the same as the one for compressible elasticity (ν not too close to 0.5).

The next example investigates the effect of increasing H/δ while fixing $N = 16$ and $H/h = 120$. The results on the left half of Table 7.3 are also plotted in Figure 7.3.

TABLE 7.3
Two-dimensional results for $N = 16$, $H/h = 120$, and increasing values of H/δ.

| H/δ	structured decomposition				unstructured decomposition			
	$\nu = 0.3$		$\nu = 0.4999$		$\nu = 0.3$		$\nu = 0.4999$	
	iter	cond	iter	cond	iter	cond	iter	cond
4	31	11.0	37	17.2	33	9.61	38	16.2
5	33	11.9	39	19.3	35	10.5	40	19.0
6	34	12.6	42	21.0	36	11.4	43	21.3
10	39	14.9	50	32.4	41	14.4	52	33.8
12	41	16.3	57	42.9	43	15.8	59	45.5
15	44	18.4	70	69.3	45	19.1	71	71.9
20	48	21.8	98	142	49	20.8	90	121
30	56	31.9	163	424	56	28.5	144	317
40	63	42.1	> 200	945	64	37.3	> 200	673
60	75	62.4	> 200	2.83e3	78	55.1	> 200	2.02e3
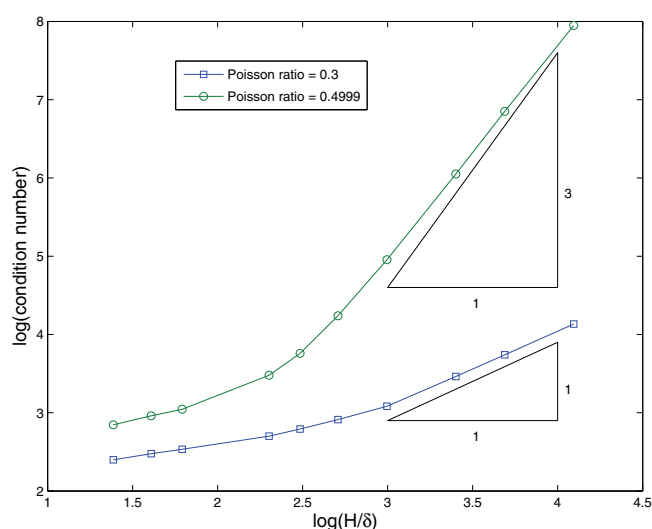
FIG. 7.3. *Two-dimensional results from Table 7.3.*

Notice that the results are fundamentally different for the compressible ($\nu = 0.3$) and almost incompressible cases. For compressible materials, condition number estimates appear to be proportional to H/δ, whereas for almost incompressible materials the growth is much larger and closer to the estimate of $(H/\delta)^3(1 + \log(H/\delta))$ in Theorem 4.1.

Another difference for compressible and almost incompressible materials is shown in Table 7.4. Here we see for a minimal overlap ($\delta/H = 0$) that the condition number estimates for almost incompressible materials grow without bound as the Poisson ratio approaches 0.5. Thus, for such materials, one should use an overlap no smaller than the element length h.

The next example is for a problem with discontinuous material properties. In a centered square region of length $1/2$, the elastic modulus $E = \sigma$ and the Poisson ratio $\nu = 0.3$. For the remaining part of the domain, $E = 1$ and $\nu = 0.49999$. For values of $\sigma \gg 1$, this can be viewed as a model of a steel component embedded in a softer, but almost incompressible, material such as rubber. Because the subdomain boundaries are aligned with material boundaries for the structured decomposition, condition number estimates in Table 7.5 are bounded independently of σ as the theory

TABLE 7.4

Two-dimensional results for a structured decomposition of 16 subdomains with $H/h = 8$.

ν	$\delta/H = 1/4$		$\delta/H = 1/8$		$\delta/H = 0$	
	iter	cond	iter	cond	iter	cond
0.3	25	8.05	29	10.0	36	19.4
0.4	27	8.21	31	11.4	42	23.9
0.49	29	10.0	36	16.3	70	66.8
0.499	30	10.5	37	17.4	108	142
0.4999	31	10.6	39	17.6	> 200	526
0.49999	33	10.6	40	17.6	> 200	4.12e3

TABLE 7.5

Two-dimensional results for a problem with discontinuous material properties. Fixed values of $N = 16$, $H/h = 16$, and $H/\delta = 4$ are used.

σ	structured decomposition		unstructured decomposition	
	iter	cond	iter	cond
10^{-4}	35	10.3	36	11.0
10^2	34	10.3	34	10.7
1	36	11.7	35	11.9
10^2	34	14.7	40	25.4
10^4	32	14.9	43	149

TABLE 7.6

Three-dimensional results for $H/h = 8$, $H/\delta = 4$, and increasing numbers of subdomains N. The number of unknowns for the example with 216 subdomains exceeds 2.5 million.

N	structured decomposition						unstructured decomposition					
	$\nu = 0.3$		$\nu = 0.4999$		$\nu = 0.49999$		$\nu = 0.3$		$\nu = 0.4999$		$\nu = 0.49999$	
	iter	cond	iter	cond	iter	cond	iter	cond	iter	cond	iter	cond
27	33	15.4	44	25.0	44	25.0	36	12.9	44	23.1	46	23.2
64	36	17.7	48	27.3	49	27.4	39	15.5	47	25.3	50	25.3
125	39	19.3	50	28.9	53	29.0	43	17.8	50	27.9	51	27.9
216	41	20.5	52	31.1	55	31.3	47	21.2	53	32.7	54	32.7

TABLE 7.7

Three-dimensional results for $N = 27$, $H/\delta = 4$, and increasing values of H/h.

H/h	structured decomposition						unstructured decomposition					
	$\nu = 0.3$		$\nu = 0.4999$		$\nu = 0.49999$		$\nu = 0.3$		$\nu = 0.4999$		$\nu = 0.49999$	
	iter	cond	iter	cond	iter	cond	iter	cond	iter	cond	iter	cond
4	32	13.7	40	19.7	40	19.7	35	12.9	43	21.7	44	21.7
8	33	15.4	44	25.0	44	25.0	35	12.8	43	23.5	44	23.5
12	35	16.3	44	28.1	46	28.1	38	14.7	50	29.0	51	29.0

implies. In contrast, some of the unstructured subdomains contain two different materials, and condition number estimates continue to grow with increasing values of σ.

7.2. Three dimensions. The numerical examples in this section mirror their two-dimensional counterparts of the previous section. Compared to two-dimensional cases, the subdomain matrix factorizations in three dimensions may require significantly more computational resources. Thus, attention is restricted to problems in which the ratio H/h is no larger than 12. The potentially large computational requirements of direct solvers in three dimensions highlights the need for algorithms which use inexact solutions of the local

TABLE 7.8
Three-dimensional results for $N = 27$, $H/h = 12$, and increasing values of H/δ.

H/δ	structured decomposition				unstructured decomposition			
	$\nu = 0.3$		$\nu = 0.4999$		$\nu = 0.3$		$\nu = 0.4999$	
	iter	cond	iter	cond	iter	cond	iter	cond
4	35	16.3	44	28.1	35	12.9	43	21.7
6	38	20.8	51	34.8	41	16.4	51	31.1
12	51	30.7	86	123	47	21.5	74	71.2

TABLE 7.9
Three-dimensional results for a problem with discontinuous material properties. In a centered cube region of dimension $1/3$, the elastic modulus equals σ and the Poisson ratio is 0.3. For the remainder of the region, the elastic modulus is unity and the Poisson ratio is 0.49999. Fixed values of $N = 27$, $H/h = 8$, and $H/\delta = 4$ are used.

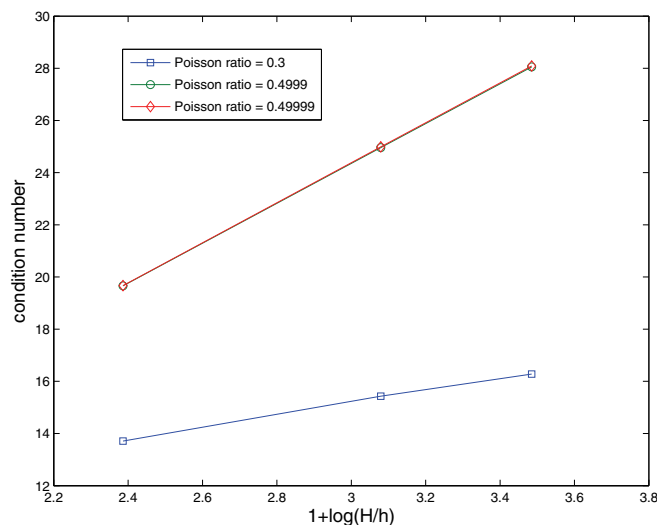| σ	structured decomposition		unstructured decomposition	
	iter	cond	iter	cond
10^{-4}	44	22.0	45	21.3
10^2	43	22.0	44	21.3
1	45	23.8	45	22.6
10^2	47	27.5	63	55.7
10^4	46	27.7	83	201

FIG. 7.4. *Three-dimensional results from Table 7.7.*

subdomain problems and quite possibly the global coarse problem as well. Such inexact methods will be the topic of a future investigation.

Results shown in Tables 7.6–7.9 and Figure 7.4 exhibit the same trends that were observed for the two-dimensional examples. Compared with the two-dimensional examples, we were not able to generate numerical results for as large of values of H/h. Nevertheless, results in Figure 7.4 are consistent with a condition number bound proportional to $1 + \log(H/h)$ for fixed values of H/δ, as was the case in two dimensions. As before, a much stronger dependence on the ratio H/δ is evident in Table 7.8 for almost incompressible materials.

REFERENCES

[1] G. Acosta, R. G. Durán, and M. A. Muschietti, *Solutions of the divergence operator on John domains*, Adv. Math., 206 (2006), pp. 373–401.
[2] O. Axelsson, *Preconditioning of indefinite problems by regularization*, SIAM J. Numer. Anal., 16 (1979), pp. 58–69.
[3] M. Benzi and M. A. Olshanskii, *An augmented Lagrangian-based approach to the Oseen problem*, SIAM J. Sci. Comput., 28 (2006), pp. 2095–2113.
[4] M. Bhardwaj, G. Reese, B. Driessen, K. Alvin, and D. Day, *Salinas—an implicit finite element structural dynamics code developed for massively parallel platforms*, in Proceedings of the 41st AIAA/ASME/ASCE/AHS/ASC SDM conference, Atlanta, GA, AIAA, 2000, pp. 2000-1651.
[5] D. Boffi and L. Gastaldi, *On the quadrilateral Q_2-P_1 element for the Stokes problem*, Internat. J. Numer. Methods Fluids, 39 (2002), pp. 1001–1011.
[6] B. Bojarski, *Remarks on Sobolev imbedding inequalities*, in Complex Analysis, Joensuu 1987, Lecture Notes in Math. 1351, Springer, Berlin, 1988, pp. 52–68.
[7] J. H. Bramble, *A proof of the inf-sup condition for the Stokes equations on Lipschitz domains*, Math. Models Methods Appl. Sci., 13 (2003), pp. 361–371.
[8] S. C. Brenner and R. Scott, *The Mathematical Theory of Finite Element Methods*, 3rd ed., Springer, Berlin, Heidelberg, New York, 2008.
[9] F. Brezzi and M. Fortin, *Mixed and Hybrid Finite Element Methods*, Springer Ser. Comput. Math. 15., Springer, New York, 1991.
[10] S. Buckley and P. Koskela, *Sobolev-Poincaré implies John*, Math. Res. Lett., 2 (1995), pp. 577–593.
[11] M. A. Casarin, *Schwarz Preconditioners for Spectral and Mortar Finite Element Methods with Applications to Incompressible Fluids*, Ph.D. thesis, Dept. of Mathematics, Courant Institute of Mathematical Sciences, New York University, 1996; Technical report 717, Department of Computer Science, Courant Institute.
[12] A. C. de Niet and F. W. Wubs, *Two preconditioners for saddle point problems in fluid flows*, Internat. J. Numer. Methods Fluids, 54 (2007), pp. 355–377.
[13] M. Dobrowolski, *On the LBB constant on stretched domains*, Math. Nachr., 254–255 (2003), pp. 64–67.
[14] C. R. Dohrmann, A. Klawonn, and O. B. Widlund, *A family of energy minimizing coarse spaces for overlapping Schwarz preconditioners*, in Proceedings of the 17th International Conference on Domain Decomposition Methods in Science and Engineering, Strobl, Austria, 2006, Lect. Notes Comput. Sci. Eng. 60, U. Langer, M. Discacciati, D. Keyes, O. Widlund, and W. Zulehner, eds., Springer, Berlin, 2007, pp. 247–254.
[15] C. R. Dohrmann, A. Klawonn, and O. B. Widlund, *Domain decomposition for less regular subdomains: Overlapping Schwarz in two dimensions*, SIAM J. Numer. Anal., 46 (2008), pp. 2153–2168.
[16] C. R. Dohrmann and R. B. Lehoucq, *A primal-based penalty preconditioner for elliptic saddle point systems*, SIAM J. Numer. Anal., 44 (2006), pp. 270–282.
[17] C. R. Dohrmann, *Preconditioning of saddle point systems by substructuring and a penalty approach*, in Domain Decomposition Methods in Science and Engineering XVI, Proceedings of the 16th International Conference on Domain Decomposition Methods, New York City, 2005, Lect. Notes Comput. Sci. Eng. 55, D. E. Keyes and O. B. Widlund, eds., Springer, Berlin, 2006, pp. 53–64.
[18] M. Dryja, B. F. Smith, and O. B. Widlund, *Schwarz analysis of iterative substructuring algorithms for elliptic problems in three dimensions*, SIAM J. Numer. Anal., 31 (1994), pp. 1662–1694.
[19] R. G. Durán and M. A. Muschietti, *The Korn inequality for Jones domains*, Electron. J. Differential Equations, 2004 (2004), pp. 1–10.
[20] V. Girault and P.-A. Raviart, *Finite Element Methods for Navier-Stokes Equations, Theory and Algorithms*, Springer Ser. Comput. Math. 5, Springer, Berlin, 1986.
[21] P. Goldfeld, L. F. Pavarino, and O. B. Widlund, *Balancing Neumann-Neumann preconditioners for mixed approximations of heterogeneous problems in linear elasticity*, Numer. Math., 95 (2003), pp. 283–324.
[22] P. W. Jones, *Quasiconformal mappings and extendability of functions in Sobolev space*, Acta Math., 147 (1981), pp. 71–88.
[23] G. Karypis and V. Kumar, *METIS Version* 4.0, University of Minnesota, Department of Computer Science, Minneapolis, MN, http://glaros.dtc.umn.edu/gkhome/metis/metis/overview (1998).

[24] A. KLAWONN AND L. F. PAVARINO, *Overlapping Schwarz methods for mixed linear elasticity and Stokes problems*, Comput. Methods Appl. Mech. Engrg., 165 (1998), pp. 233–245.

[25] A. KLAWONN AND L. F. PAVARINO, *A comparison of overlapping Schwarz methods and block preconditioners for saddle point problems*, Numer. Linear Algebra Appl., 7 (2000), pp. 1–25.

[26] A. KLAWONN, O. RHEINBACH, AND O. B. WIDLUND, *An analysis of a FETI–DP algorithm on irregular subdomains in the plane*, SIAM J. Numer. Anal., 46 (2008), pp. 2484–2504.

[27] A. KLAWONN AND O. RHEINBACH, *Robust FETI-DP methods for heterogeneous three dimensional linear elasticity problems*, Comput. Methods Appl. Mech. Engrg., 196 (2007), pp. 1400–1414.

[28] A. KLAWONN AND O. B. WIDLUND, *Dual-primal FETI methods for linear elasticity*, Comm. Pure Appl. Math., 59 (2006), pp. 1523–1572.

[29] J. LI AND O. WIDLUND, *BDDC algorithms for incompressible Stokes equations*, SIAM J. Numer. Anal., 44 (2006), pp. 2432–2455.

[30] J. LI, *A dual-primal FETI method for incompressible Stokes equations*, Numer. Math., 102 (2005), pp. 257–275.

[31] J. MANDEL, *Iterative solvers by substructuring for the p-version finite element method*, Comput. Methods Appl. Mech. Engrg., 80 (1990), pp. 117–128.

[32] J. NEČAS, *Les Méthodes Directes en Théorie des Équations Elliptiques*, Academia, Prague, 1967.

[33] B. F. SMITH, P. BJØRSTAD, AND W. GROPP, *Domain Decomposition: Parallel Multilevel Methods for Elliptic Partial Differential Equations*, Cambridge University Press, New York, 1996.

[34] R. STENBERG, *A technique for analysing finite element methods for viscous incompressible flow*, Internat. J. Numer. Methods Fluids, 11 (1990), pp. 935–948.

[35] A. TOSELLI AND O. WIDLUND, *Domain Decomposition Methods—Algorithms and Theory*, Springer Ser. Comput. Math. 34, Springer, Berlin, Heidelberg, New York, 2005.